



University of  
**BRISTOL**

**School of Chemistry**

Using Nanostructured Surfaces as Bactericides

Phillipa Taylor

**This thesis is submitted in partial fulfilment of the requirements for the Honours  
Degree of MSci at the University of Bristol**

Supervisor: Professor Paul May

Second Assessor: Professor Neil Fox

Physical and Theoretical Group

# Abstract

---

Antibiotics are widely used to treat bacterial infections. Recently however, more multi-drug resistance strains of bacteria have been evolving, where antibiotics are less effective at killing them. Hence there is a need to for a paradigm-shifting idea to combat antibiotic resistance.

Antibiofouling surfaces are natural and artificial surfaces that have nanostructures able to kill bacteria *via* a non-specific physical mechanism, rather than the specific chemical mechanism of antibiotics. This non-specific mechanism is much more invasive to bacteria so that developing resistance is much more difficult. These surfaces have the potential to be used as antibacterial surfaces in a variety of medical applications including implants.

Using the gram-negative, motile bacteria *E. coli* [K12] the nanostructured surface black silicon (bSi) was confirmed to have bactericidal properties. The aim of the project however, was to study which characteristics of the surface are most important to its antibacterial ability.

The reactive ion etching (RIE) process, by which bSi is fabricated, can be varied producing long, intermediate and short needled bSi, each with differing needle length, tip diameter and spike density. A thin diamond film successfully coated the long needled bSi, by hot filament chemical vapour deposition (HFCVD), to increase wettability, tip diameter and resilience of the needles. The surfaces were analysed by scanning electron microscopy and Raman spectroscopy.

*E. coli* was incubated on the surface for 1 hr and the long, intermediate, short and diamond coated bSi needles had a cell death percentage of 23%, 30%, 31 %, and 20%, respectively.

Experiments demonstrate that cell adhesion does not have an effect on the cell death percentage, whereas increasing the tip diameter and decreasing spike density are both detrimental to the effectiveness of the needles.

A 0.4  $\mu\text{L}/\text{mL}$  aqueous solution of polyDADMAC was successfully added to the surface of the long needled bSi which presented a synergic chemical and physical killing mechanism against *E. coli* with a cell death percentage of 54%.

The short needled bSi surfaces were unsuccessful against the gram-positive, non-motile bacteria *S. gordonii* [DL1] with only a 0.23% increase in cell death percentage compared to the flat silicon control.

These characteristics may be applicable to a variety of nanostructured surfaces in order to increase their antibacterial properties.

# Acknowledgements

---

Firstly, I would like to express my gratitude to Dr Gavin Hazell of the school of Oral and Dental Sciences, who has given me so much of his time and support to introduce me to microbiology. His guidance has been invaluable and without it I would have been unable to carry out this project.

I would also like to thank to my supervisor, Professor Paul May, for his enthusiasm and innovative ideas throughout the project. I would also like to extend my thanks to my second assessor, Professor Neil Fox, who also offered inventive ways to tackle problems which inevitably arose.

Finally, I would like to thank everyone in the diamond and biomaterials research groups, especially Alexander Croot, Edward Mahoney, Fabian Fogarty and Michael James for all their help, insight and always managing to keep our spirits high.

# Table of Contents

---

1	Introduction .....	6
1.1	Implantation Devices/ Need for Antibacterial Surfaces .....	6
1.2	Infection of Implants.....	6
1.3	Antibiotics.....	7
1.4	Bactericidal Nanostructures in Nature .....	8
1.5	Bacteria Cell Wall Structure.....	10
1.5.1	Stretching Theory .....	11
1.5.2	Cellular Adhesion .....	12
1.6	Biomimetic Bactericidal Nanostructures .....	13
1.7	Black Silicon .....	15
1.7.1	Varying the Height of bSi Needles .....	16
1.7.2	Diamond Coating bSi .....	16
1.7.3	Addition of Polymers to bSi .....	17
1.8	Project Objectives.....	17
2	Method and Materials .....	19
2.1	Fabrication of Surfaces .....	19
2.1.1	Fabrication of bSi.....	19
2.1.2	Diamond Coating bSi.....	20
2.1.3	Polymer Coating bSi.....	20
2.2	Determining Surface Energy.....	21
2.3	Antibacterial Surface Testing.....	21
2.3.1	Bacterial Culture Preparation.....	21
2.3.2	Preparation for SEM .....	22
3	Results.....	23
3.1	Surface Analysis .....	23
3.1.1	Uncoated bSi .....	23
3.1.2	Polymer Coated bSi .....	27
3.1.3	Surface Energy .....	29
3.2	Live/Dead Assay .....	31
3.2.1	Uncoated bSi.....	32
3.2.2	Diamond Coated bSi.....	35
3.2.3	Polymer Coated bSi .....	36
3.2.4	<i>S. gordonii</i> .....	38

4	Discussion.....	39
4.1	Live/Dead Assays.....	39
4.2	Physical Killing Mechanism.....	39
4.3	The Relationship between Surface Topography/Chemistry and Cell Death Percentage 42	
4.3.1	Adhesion.....	42
4.3.2	Tip Diameter.....	42
4.3.3	Spike Density.....	43
4.3.4	Polymer Coating.....	44
4.3.5	<i>E. coli</i> versus <i>S. gordonii</i> .....	46
5	Conclusions.....	47
5.1	Adhesion.....	47
5.2	Tip Diameter.....	47
5.3	Length of Needles.....	48
5.4	Spike Density.....	48
5.5	PolyDADMAC.....	48
5.6	<i>S. gordonii</i> .....	49
6	Further Work.....	50
7	References.....	51

# 1 Introduction

---

## 1.1 Implantation Devices/ Need for Antibacterial Surfaces

Medical implants are a huge part of medicine that span over multiple fields. Devices range from being small/simple like catheters and dental implants to more complex devices such as joint replacements and mechanical heart valves. It has been estimated that everyone in our modern society will have at least one medical implant in their lifetime.[1], [2]

With an aging population, orthopaedic implants are becoming much more popular with over 2.6 million patients having joint prostheses and fracture-fixation devices inserted last year. From these, approximately 112,000 presented with an infection leading to an average cost of \$45,000 per patient, in the U.S., for their medical and surgical treatment. [3]

Catheter insertion has become one of the most common practices due to their variety of purposes; hemodynamic monitoring, renal replacement therapy, nutritional support and medication administration. First used in 1929, now over 150 million of these intravascular devices are used every year in the U.S. Even though catheter insertion is less invasive than joint replacement surgery, complications still occur most common being bloodstream infections which end up costing the U.S. government between \$670 million- \$2.68 billion a year. [4]

With an ageing population, coupled with an increase in prosthetic joint replacement, demand for biomedical implants is at an all-time high. [1]

## 1.2 Infection of Implants

An infected implant can be caused by a colony of fewer than 100 bacteria which exponentially grow once inside the body [5] . This, in turn, can lead to failure of the implant, a systemic infection, septicemia, and in some cases even death. [6], [7]

One of the highest risks associated with medical implants is bacterial infection and they are notoriously difficult to eradicate for two main reasons:

First, when an implant is introduced into a host, the body's response is to cover the foreign object in plasma proteins, in a process known as biointegration. This protein layer encourages cell adhesion and tissue regrowth to promote wound repair. However these proteins are not cell specific and can also promote bacterial cell adhesion and colonisation. This is known as the 'race to the surface' scenario. [5]

Second, once a biofilm has been fully established on the implant's surface, extracellular polymers are expelled from the bacteria. These polymers simultaneously entrap the bacteria onto the surface, making cell adhesion irreversible, as well as acting as a defence mechanism by inhibiting the immune system from attacking. [8]

The only certain way of eradicating the infection is to remove the implant and any infected tissue surrounding it and replace the implant with a temporary spacer loaded with antibiotic. Only after all the infection has been eradicated, which is a minimum of 6 weeks, can the implant be permanently replaced [5]. Overall this requires a lot of time, money and endurance on the patient's behalf.

### **1.3 Antibiotics**

The first antibiotic, Penicillin, was revolutionary in the 1940s but since then bacteria are continuously evolving to counteract the antibacterial effects [9]. This results in the need for pharmaceutical companies to constantly invent new bactericidal compounds to compete with these evolutions. However, little research is being done to combat resistance due to the small return on investment.

There are three main mechanisms through which bacteria become multidrug resistant. First, the main contributor to resistance is the increase in efficiency of expelling the antibiotic from the cell by upgrading their efflux pumps. Second, antibiotics have a high binding affinity to target proteins found inside the cell, these can be modified directly or protected by another protein to decrease the binding affinity and lessen the effectiveness of the antibiotic. Thirdly, the antibiotic can be degraded directly through enzymes found in the cell *via* hydrolysis mechanisms or transference of a chemical group *i.e.* an acyl or phosphate group to prevent the attachment by steric hindrance of the antibiotic to a protein. [10], [11]

The two most powerful antibiotics to date are methicillin and vancomycin, but even these have been proven ineffective against some strains of *Staphylococcus aureus* (MRSA) and *Enterococcus* (VRE). Additionally, these strains of bacteria are not uncommon; 40% of bacteria collected in hospitals were found to be different strains of MRSA. [9]

Furthermore, the centre of a bacterial colony has a lower level of nutrients and so bacteria found here become metabolically inactive and are hard to penetrate. Under these circumstances, even with antibiotic concentrations 20 to 100 times more than the minimal inhibition concentration, bacteria in the centre do not uptake any of the antibiotic leading to the persistence of the biofilm [5], [7]. Moreover, there are some serious side effects associated with antibiotics including

toxicity to the kidneys, brain, neural and skeletal muscles, liver impairment and in a small number of cases allergic reactions. [12]

Failure in combating antimicrobial resistance may lead to an additional 10 million lives being lost by 2050 due to drug resistant strains of bacteria, overtaking the number of combined deaths from all types of cancer. This would cost the global economy \$100 trillion and demonstrates the need for a paradigm-shift. [13]

#### **1.4 Bactericidal Nanostructures in Nature**

From an evolutionary stance, many living organisms have developed antibiofouling and self-cleaning properties [14], for example the wings of the cicada (*Psaltodo claripennis*) [15], shark skin (*Isurus oxyrinchus*) [16], and lotus leaves (*Nelumbo nucifera*) [18] *etc.* to avoid the build-up of biological matter which can cause infections [15], [19].

Self-cleaning biological surfaces normally have physical properties which increase hydrophobicity and in some circumstances can even become superhydrophobic [20]. Sharklet AF™ micropattern technology mimics shark skin which is known for its self-cleaning properties. The skin is covered in microgrooves similar in size to bacteria thus hindering their attachment. Studies have shown the inhibition of growth of the bacteria *Staphylococcus aureus*, and *Pseudomonas aeruginosa*. [21], [22]

While investigating the bactericidal nature of cicada (*Psaltodo claripennis*) wings, Hasan *et al.* [23] found them to also have antibiofouling properties. The gram-negative bacteria, *P.aeruginosa*, were killed within approximately 3 mins of exposure to the surface. There was a minor effect in the antibiofouling nature even after the surface had been coated in a thin layer of gold suggesting the bacteria were killed by a purely physical mechanism.

Under scanning electron microscopy (SEM) the cicada wings were found to be covered in a regular arrangement of nanopillars formed from proteins, chitin and cuticular waxes which mechanically ruptured the bacteria. These nanopillars measure 200 nm tall, 100 nm in diameter at the base and 60 nm at the top and were 170 nm apart, as shown in Figure 1.1 SEM image of the cicada (*Psaltodo claripennis*) wing shows the surface is covered in a regular array of nanopillars. [15]

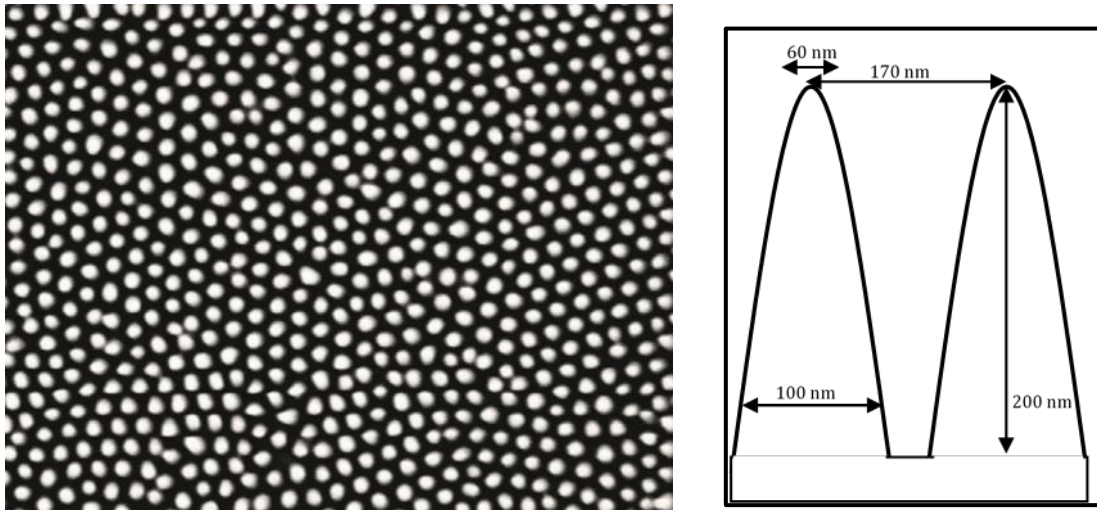


Figure 1.1 SEM image of the cicada (*Psaltoda claripennis*) wing shows the surface is covered in a regular array of nanopillars. [23]

Further studies by Hasan *et al.* [24] showed the surface of the cicada wing were consistently effective at killing the gram-negative bacteria; *Branhamella catarrhalis*, *E. coli*, *P. aeruginosa*, and *Pseudomonas fluorescens*. However they were less effective against the gram-positive bacteria; *Bacillus subtilis*, *Planococcus maritimus*, and *Staphylococcus aureus*.

A similar study by Ivanova *et al.* [25] found that under SEM, shown in Figure 1.2, the surface of the wings of the dragonfly (*Diplacodes bipunctata*) displayed a disordered array of similarly shaped nanopillars, with a height of 240 nm. These were highly bactericidal against gram-negative *P. aeruginosa*, gram-positive *S. aureus*, and both the vegetative cells and spores of *Bacillus subtilis*, with an estimated killing rate of 450,000 cells  $\text{min}^{-1} \text{cm}^{-2}$ .

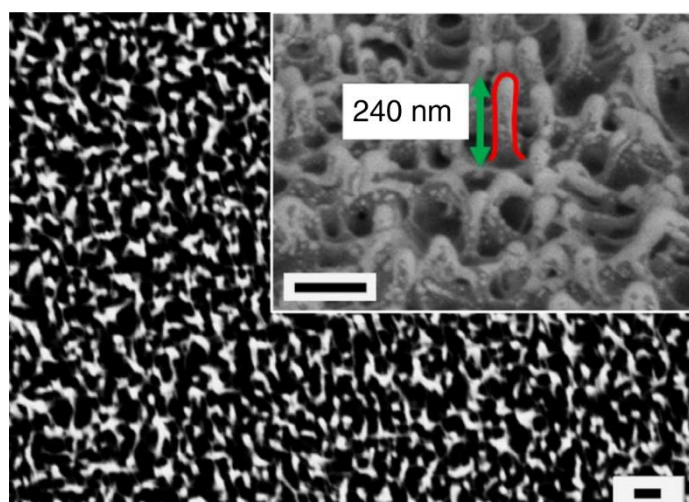


Figure 1.2. An SEM image of the surface of the dragonfly (*Diplacodes bipunctata*) wing at x35,000 magnification [25]

These nanopillars are not effective at repelling bacteria but in fact have an “attachment/killing cycle” of approximately 20 mins, where the bacteria attach, rupture, and disperse [15]. The dispersion of the bacteria involves either the bacteria sinking down between the needles or detaching from the surface all together.

## 1.5 Bacteria Cell Wall Structure

Bacteria are split in to two classes; gram-positive and gram-negative. Both classes contain a phospholipid cell membrane and a murein (also known as peptidoglycan) cell wall. Murein is a chain made up of two alternating sugar derivatives; *N*-acetylglucosamine (NAG) and *N*-acetylmuramic (NAM). Amino acids such as L-alanine and D-glutamic acid form side chains by attaching to the sugar polymer and can cross-link with each other. [26]

Most gram-positive bacteria have a single thick layer of murein ranging from 20-80 nm thick, as shown in Figure 1.3. (a). The amino acid side-chains are interlinked through a glycine pentapeptide interbridge.

In contrast, most gram-negative bacteria have a much thinner, more elasticated cell wall than gram-positive bacteria, being approximately 5-10 nm thick. The cell wall is made up of three layers: the phospholipid cell membrane; a thin layer of murein suspended in the periplasmic space; and an outer membrane. The cross-linkage of murein chains in gram-negative bacteria contains a direct interbridge between amino acid side chains leading to more closely packed systems. The outer membrane is mainly made up of polyanionic lipopolysaccharides (LPS), shown in Figure 1.3 (b). Gram-negative bacteria are more inclined to become antibiotic resistant than gram-positive bacteria due to the additional outer membrane acting as an additional barrier to antibiotics. [9], [26], [27]

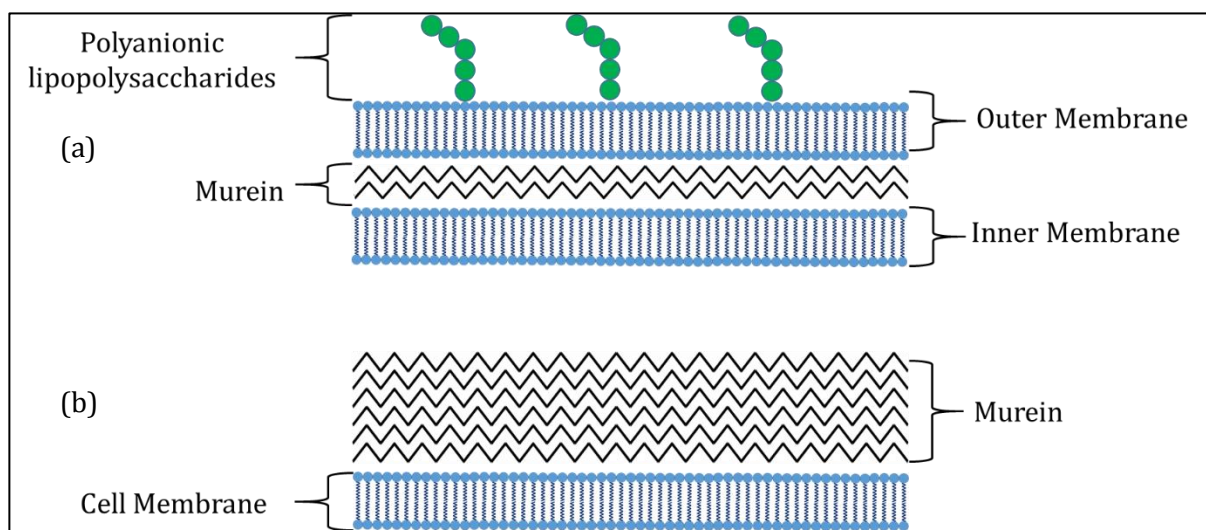


Figure 1.3. The cell wall structure of (a) gram-negative and (b) gram-positive bacteria.

A combination of the anionic phosphate groups found in the cell membrane and the polyanionic lipopolysaccharides give the cell wall a net negative charge.

Depending on the bacteria the overall structure of the cell wall may include an array of folds, receptors and protrusions called *microvilli*, *lamellipodia* and *filopodia*, which have been found to contribute to the adhesion of the cell to a surface. [28]

### 1.5.1 Stretching Theory

The nanopillars found on the cicada wings are dimensionally much larger than the cell wall and surface nanostructures found in bacteria. Therefore, this system can be represented in computational studies as a simple elastic layer which ruptures after applying a set amount of force *via* ‘the stretching theory’.

Xue *et al.* [29] have designed a mathematical ‘stretching theory’ model that possibly explains the bactericidal nature of the nanostructured surfaces, like the cicada wing. As demonstrated in Figure 1.4, by calculating the difference in surface area of the cell wall adhered to a pillar ( $S_A$ ) and that suspended between two pillars ( $S_B$ ), the stretching degree can be calculated. If the stretching degree exceeds the threshold of the elastic layer the cell wall will rupture.

Xue *et al.* [29] also identified that other interactions must also have a part in rupturing the cell, otherwise the stretching threshold cannot be overcome. Since the rupturing mechanism is purely physical it is safe to assume that no specific (i.e. ligand-receptor) interactions are involved in rupturing the bacteria. Non-specific interactions must, therefore, have some part in the physical mechanism. These include van der Waals, electrostatic, steric and gravitational interactions, and solvation forces. [30]

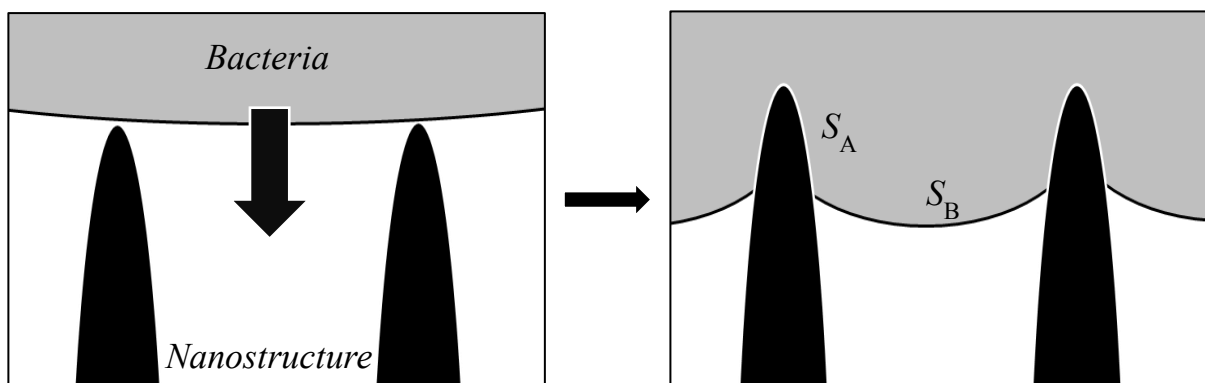


Figure 1.4. By comparing the surface area of the cell wall which has adhered to the pillar ( $S_A$ ) and that suspended between two pillars ( $S_B$ ), the stretching degree can be calculated.

### 1.5.2 Cellular Adhesion

A solid surface, when inspected with the naked eye, has only a simply defined profile. When the same surface is viewed under low magnification, i.e. an optical microscope, new features will be seen and the topography can be described as ‘surface waviness’. If the surface is viewed under further magnification, i.e. using an atomic force microscope (AFM), even more of the structure can be seen. This is the same scale as bacteria and the topography can be described as ‘surface roughness’. Surface roughness,  $\tilde{h}$ , can be quantified by simplifying a surface’s profile to be a sinusoidal wave, where  $\tilde{h}$  is the vertical distance between the highest and lowest points. [29], [30]

Decuzzi and Ferrari [31] designed a mathematical model to show how cellular adhesion to an inert surface varies as a function of substrate roughness. Three systems with different degrees of the dimensionless surface energy ( $\tilde{\gamma}$ ):

- For a low surface energy, any roughness is detrimental to cellular adhesion ( $\tilde{\gamma} \approx 2 \times 10^{-4}$ )
- For an intermediate surface energy, roughness has a minor effect on cellular adhesion ( $\tilde{\gamma} \approx 2 \times 10^{-2}$ )
- For a high surface energy an optimal roughness can be identified ( $\tilde{\gamma} \approx 1 \times 10^{-1}$ )

These scenarios are demonstrated below in Figure 1.5..Where the surface energy ratio ( $\gamma_{\text{eff}}/\gamma_0$ ) is used to quantify the impact of topography on the strength of adhesion and is defined as the effective surface energy on a rough surface ( $\gamma_{\text{eff}}$ ) compared to that of a flat surface ( $\gamma_0$ ).

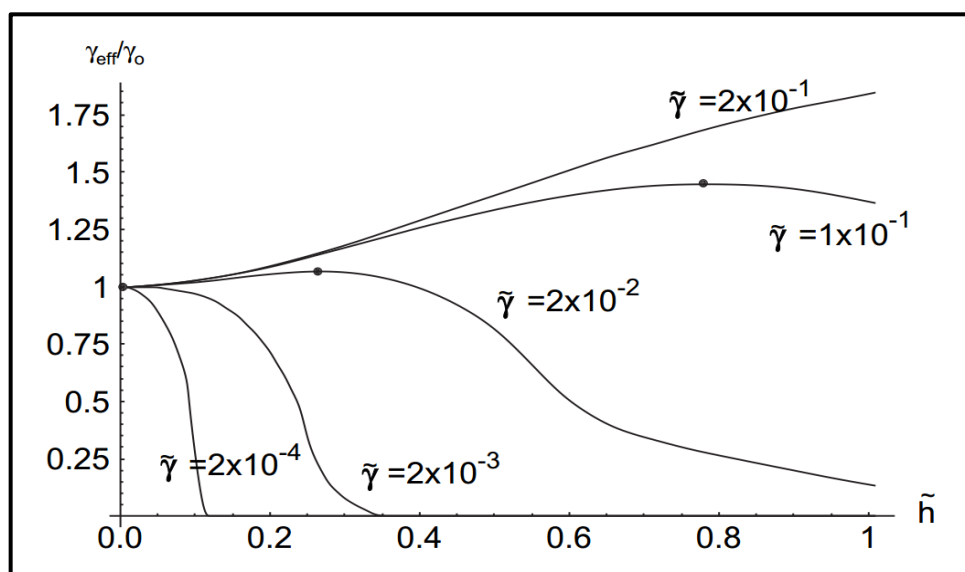


Figure 1.5. The variation of the surface energy ratio ( $\gamma_{\text{eff}}/\gamma_0$ ) as a function of roughness ( $\tilde{h}$ ) of the substrate presents three different scenarios depending on the dimensionless surface energy ( $\tilde{\gamma}$ ) [31]

Studies by Pierres *et al.* [28] found the membrane of eukaryotic monocyclic THP-1 cells on a fibronectin surface started to fluctuate at approximately 50 nm above a substrate giving the impression of the cell 'tip-toeing' in the first mins of cell-to-substrate contact before full adhesion. Bacteria are defined as prokaryotic cells and/or, unicellular microorganisms. In contrast, eukaryotic cells are found in larger organisms, such as *Homo sapiens*. Despite their difference in cell structure, prokaryotic cells have similar biological chemistry to eukaryotes and may 'tip-toe' in a similar fashion. [32]

## 1.6 Biomimetic Bactericidal Nanostructures

Antimicrobial compounds were revolutionary in their time but increasing levels of bacterial resistance does pose a significant problem for their continued use, as mentioned before. Hence the increase in topographical studies of surfaces that can kill bacteria *via* a non-specific physical mechanism rather than a specific chemical one. [15], [33]

Surfaces that mimic the cicada nanopillars are highly sought after, due to their non-specificity against bacteria. Ivanova *et al.* [25] found that black silicon (bSi) has a similar topography to dragonfly wings, as shown in Figure 1.6.. Samples of bSi with 500 nm long needles, were tested against three different bacterial species and successfully deformed and killed gram-negative *P. aeruginosa*, gram-positive *Staphylococcus aureus*, and both the vegetative cells and spores of *Bacillus subtilis*. Measurements showed that bSi presented an average killing of 450,000 cells  $\text{min}^{-1} \text{cm}^{-2}$ , similar to that of the dragonfly wing.

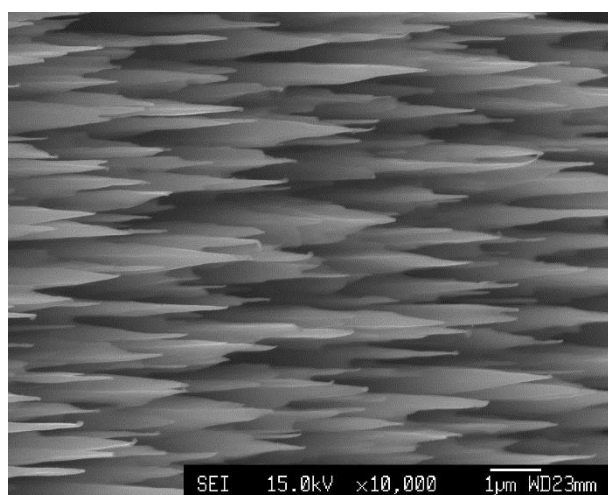


Figure 1.6. An SEM image of bSi needles which mimic the nanopillars found on the dragonfly (*Diplacodes bipunctata*) wing [34]

Similarly, Fisher *et al.* [35] found that diamond nanocones were effective at killing the gram-negative bacteria, *P. aeruginosa*. The nanocones were fabricated using microwave plasma chemical vapour deposition (MWCVD) followed by bias-assisted reactive-ion etching (RIE) by electron cyclotron resonance (ECR) deposited onto silicon wafers. Two types of nanocones were produced by varying the RIE bias, shown in Figure 1.7.

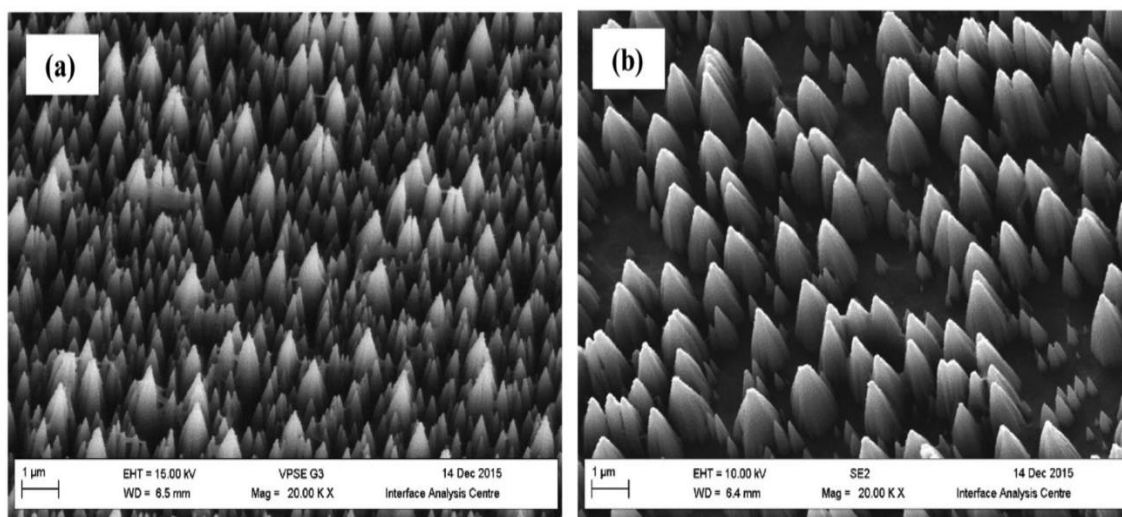


Figure 1.7. Nanocones formed from MWCVD followed by RIE are proven to be effective at killing *P. aeruginosa*. [35]

Diu *et al.* [36] engineered two types of titania ( $\text{TiO}_2$ ) patterns by applying an alkaline hydrothermal process onto a titanium surface. Using this method, the growth of titania nanowires was controlled and two topographical patterns were formed: a brush-type (Figure 1.8 (a)), and a niche-type (Figure 1.8 (b)). The bactericidal nature of these surfaces was independent on whether the bacteria were gram-negative or gram-positive, but instead was dependant on the motility of the bacteria. Motile bacteria such as *P. aeruginosa* (gram-negative) and *B. subtilis* (gram-positive) were found to be killed by these surfaces. However, the nanowires were less effective against non-motile bacteria such as *Staphylococcus aureus* (gram-positive) and *K. pneumonia* (gram-negative). The brush-type surfaces were more effective against *E. coli* but niche-type were more effective against *P. aeruginosa* and *B. subtilis*.

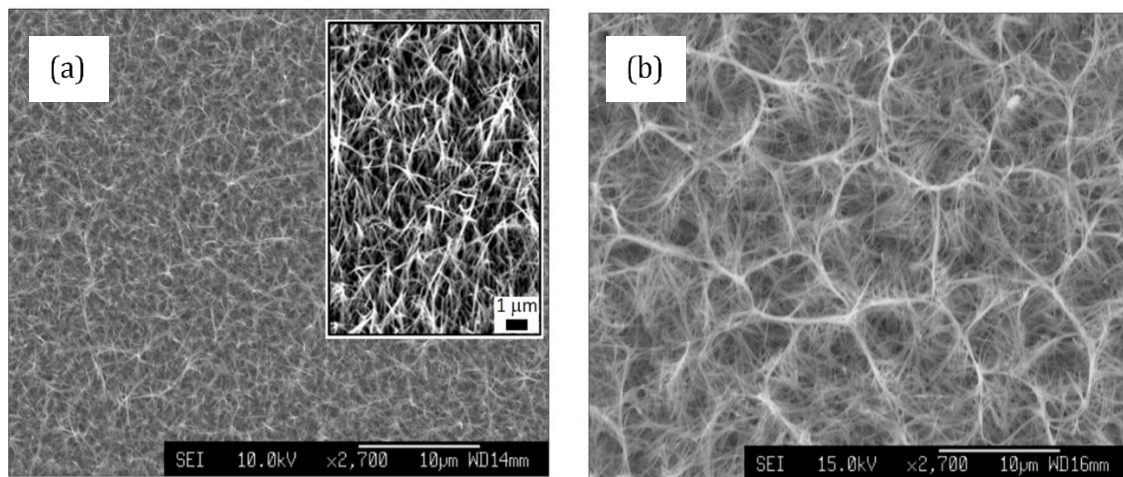


Figure 1.8. Diu *et al.* engineered two types of titania ( $\text{TiO}_2$ ) patterns; (a) brush type and (b) niche type [36].

## 1.7 Black Silicon

The high aspect ratio of bSi has created a lot of interest especially for technological applications involving energy sensing and emitting [37]. Here, bSi was first produced as a by-product of reactive-ion etching (RIE) a silicon wafer in fluorine, bromine and chlorine plasmas. Particulates from the chamber attach onto the surface acting as micromasks while etching the wafer to produce these very sharp needles, as shown in Figure 1.9. [38]

Other methods have been refined including UV and nanosphere lithography, metal-catalysed wet chemical etching and electron-beam thermal annealing, each producing bSi with variations in size, width, substrate quality and surface chemistry [25][30][38][39]

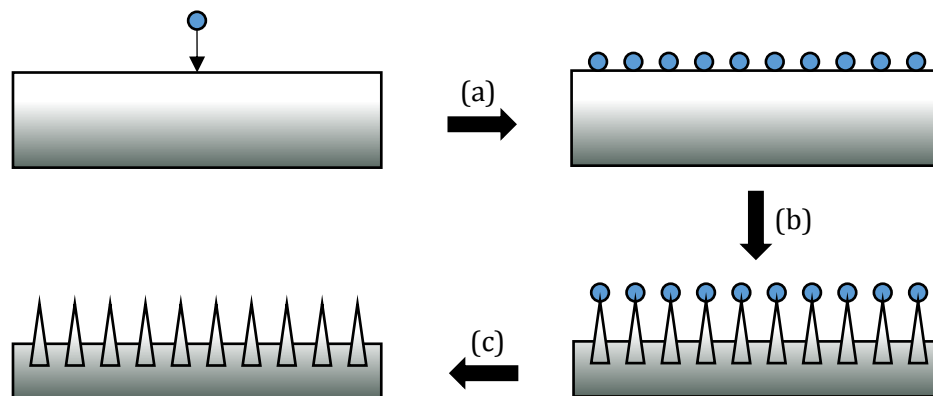


Figure 1.9. Schematic diagram demonstrating the fabrication of bSi, highlighting the following steps (a) particulates adhere to the surface and protect the surface by acting as a micromask (b) anisotropic etching of the material by the plasma gases (c) removal of the protective mask.

Cell interaction studies were carried out by Garipcan *et al.* [40] to test the biocompatibility of n-doped and undoped silicon. Using L2929 mouse fibroblast cells changes in the adhesion and morphology were tested. Results show that both surfaces had no significant cytotoxic effects thus these surfaces may be considered a viable material for biomedical implants.

Furthermore, due to the top-down synthesis and chemical inertness, the surface of bSi can be easily modified in dimensions and surface chemistry.

### **1.7.1 Varying the Height of bSi Needles**

May *et al.* [37] produced short bSi needles of length 0.5  $\mu\text{m}$ , by etching the silicon substrate with  $\text{Cl}_2\text{-O}_2$  plasma. They also produced long bSi needles of length 15-20  $\mu\text{m}$  using a cryogenic etch with  $\text{SF}_6$  and  $\text{O}_2$ .

### **1.7.2 Diamond Coating bSi**

Diamond is the only  $\text{sp}^3$  hybridised allotrope of carbon, with all other allotropes (graphite, carbon nanotubes (CNT), graphene and fullerenes) being  $\text{sp}^2$ . The  $\text{sp}^3$  tetrahedral structure in diamond is the reason why it is one of the hardest naturally occurring materials on Earth. Diamond has many outstanding properties and there is a large area of research devoted to synthesise it artificially. [41], [42], [43]

Chemical vapour deposition (CVD) is one of the most common techniques used for depositing diamond films onto solid surfaces. A mixture of gases, typically 1%vol methane in hydrogen, are activated *via* thermal activation (hot filament, HFCVD) or plasma activation (microwave plasma, MWCVD). This activation causes the molecules to dissociate into reactive radicals and atoms which nucleate onto the surface forming diamond crystals. The crystals continue to grow, homogeneously, until they coalesce forming a continuous film. [34]

May *et al.* [37] have reported that the bSi needles, mentioned above, can be coated in a thin diamond film through HFCVD. The strength and biocompatibility of the diamond make it ideal for use as a thin film to cover the bSi to make it more resilient when being used as an implant surface. [44]

### 1.7.3 Addition of Polymers to bSi

Nguyen *et al.* [45] investigated the adsorption of two human plasma proteins, albumin and fibronectin, onto bSi. Albumin is the most abundant protein in human blood plasma with a molecular weight of 66 kDa [46]. It was found that at low bulk concentrations  $<40 \mu\text{g mL}^{-1}$  the albumin proteins would accumulate between the bSi needles, while at higher concentrations albumin would 'sit' on top of the needles. Fibronectin, on the other hand, has a much higher molecular weight of 220 kDa [47] and preferred to sit on top of the needles independent of bulk concentration.

Forming polyelectrolyte layers onto potential biomedical surfaces is a common technique to modify the surface chemistry and so it may be used for clinical applications, such as enhancing cellular adhesion. Brunot *et al.* [48] studied the attachment of polyethyleneimine (PEI,  $\sim 70\text{kDa}$ ) onto Ti and TiNi alloys and their biocompatibility with osteoblast and fibroblast, cells found in the body that promote biointegration. Their findings suggested that PEI adhered to the surfaces by van der Waals forces alone, however the polymer was found to be potentially cytotoxic against osteoblasts and fibroblasts.

## 1.8 Project Objectives

The increasing number of multidrug-resistant bacteria has proven problematic, hence the growth in interest in bactericidal surfaces which can effectively kill non-specific bacteria *via* a physical mechanism instead of a chemical mechanism, since bacteria are less likely to become resistant to physical mechanisms.

Recently, bSi has been found to have bactericidal characteristics but little has been done to optimise such properties. Figure 1.10. illustrates how the surface chemistry and topography of bSi can be manipulated. In doing so, this project aims to find which of these characteristics enhance the antibacterial natures of the surface.

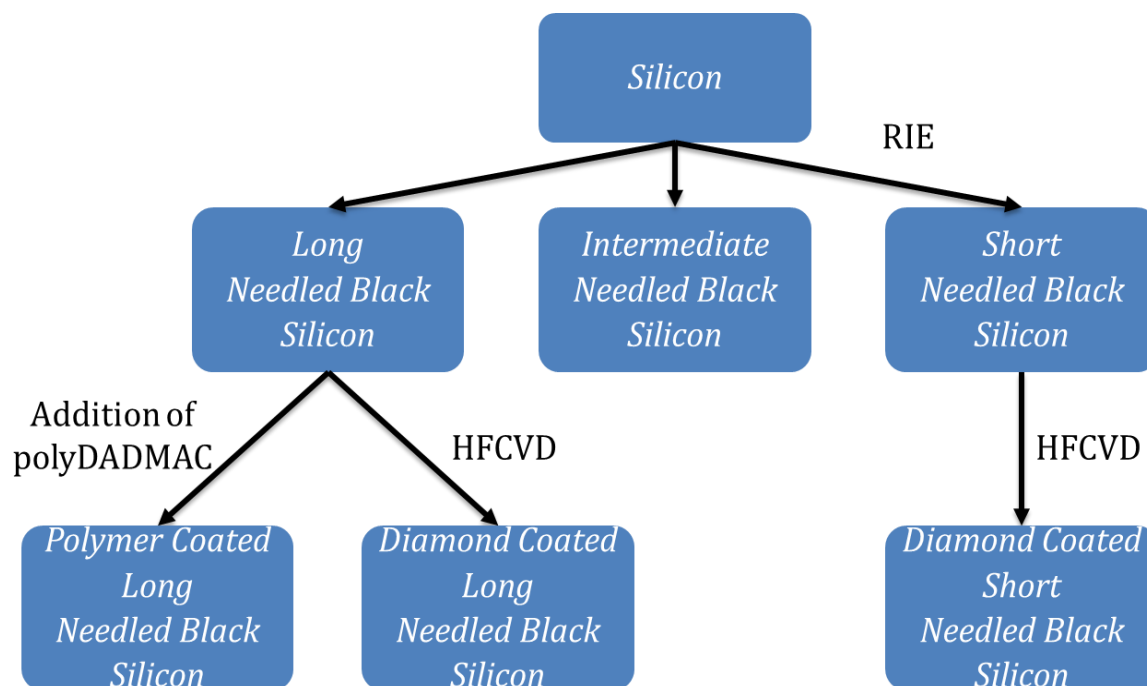


Figure 1.10. A schematic diagram illustrating how the surface chemistry and topography can be modified by RIE, HFCVD and the addition of the cationic polymer polyDADMAC.

First, the dimensions of bSi (such as needle length, tip diameter and spike density) can be varied by altering the plasma composition and etching time during the RIE process.

Second, the needles can be made more resilient to damage by adding a diamond film using HFCVD but whether or not this affects the bactericidal nature is unknown. The HFCVD process used was outlined by Clegg [34] for the short and long needled bSi.

Third, as mentioned previously, Xue *et al.* [29] calculated that the only forces acting upon the cell, leading it to rupture upon contact with the surface, are van der Waals. In the hope of increasing these forces, the cationic polymer polyDADMAC can be fixed to the surface and add an electrostatic force with the anionic bacterial cell wall. This may also aid the investigation into whether increasing total adhesion has an effect on the cell death percentage of bacteria.

## 2 Method and Materials

---

### 2.1 Fabrication of Surfaces

All of the bSi wafers were supplied by Colin Welch of Oxford Instruments Plasma Technology (Yatton, Bristol) and were prepared in the following ways.

#### 2.1.1 Fabrication of bSi

Three wafers of bSi with varying length needles were prepared by plasma etching n-doped single-crystal silicon (100) wafers under varying conditions as shown in Table 1. The difference in conditions resulted in three different lengths of bSi needles; 0.5  $\mu\text{m}$  (short), 2.5  $\mu\text{m}$  (intermediate) and 20  $\mu\text{m}$  (long).

	<b>Short bSi Needles</b>	<b>Intermediate bSi Needles</b>	<b>Long bSi Needles</b>
<b>Apparatus used</b>	Oxford Instruments System 133 fitted with an ICP380 source.	Oxford Instruments System 100 fitted with a Cobra180 ICP source	Oxford Instruments System 100 fitted with a Cobra300 ICP source.
<b>Plasma Gases</b>	Cl <sub>2</sub> (48 sccm) and O <sub>2</sub> (2 sccm) at 15 mTorr	Cl <sub>2</sub> (48 sccm) and O <sub>2</sub> (2 sccm) at 15 mTorr	SF <sub>6</sub> (60 sccm) and at O <sub>2</sub> (10 sccm) at 10 mTorr
<b>Inductively Coupled Plasma (ICP) power / W</b>	600	600	800
<b>RIE bias power / W</b>	100	50	6
<b>Electrode Temperature / °C</b>	20	20	-110
<b>Etching time / min</b>	10	20	30
<b>Additional information</b>	N/A	He at 10 Torr was applied to the backside of the sample to cool it.	He at 10 Torr was applied to the backside of the sample to cool it.

Table 1. Plasma etching silicon n-doped single-crystal silicon (100) wafers under varying conditions leads to bSi needles with varying heights.

Each wafer was cleaved into multiple 1 cm<sup>2</sup> samples using a diamond scribe.

## 2.1.2 Diamond Coating bSi

The coating method was described by May *et al.* [37].

### 2.1.2.1 Seeding

Seeding the samples with nanodiamond accelerated initial nucleation growth. The long needled bSi samples were seeded using an electrospray technique. The samples were attached using carbon adhesive pads to a grounded rotating disc using carbon adhesive pads, which rotated at  $\sim 60$  rpm. A detonation nanodiamond/methanol solution was passed through a syringe connected to a high voltage power supply (70kV). The nanodiamond/methanol solution consisted of 10 drops of NanoAmando colloid (a suspension of detonation nanodiamonds of size  $3.3 \pm 0.6$  nm suspended in water of concentration 2.0 w/v %) in  $\sim 25$  mL of methanol and was sonicated for 30 mins.

The short needled bSi samples were left unseeded to prevent the diamond layer overgrowing the needles.

Controls were fabricated by seeding p-doped single-crystal silicon (100) wafers *via* mechanical abrasion using nanodiamond grit after which the sample was washed with ethanol.

### 2.1.2.2 Hot Filament Chemical Vapour Deposition (HFCVD)

The seeded samples were then coated in boron doped diamond using a HFCVD reactor. The boron doping was to make the diamond layer electrically conducting allowing them to be potentially used for electrochemical applications, even though such electrochemical applications were not the focus of this project. The diamond coating was formed under 200, 2, and 300 sccm of hydrogen, methane and diborane respectively, at  $\sim 20$  Torr pressure and  $\sim 1000$  K, while applying a 25 A current through a Rh filament.

To prevent the diamond film from overgrowing the needles and forming a continuous flat film, the short and long needles were left to grow for 90 and 30 mins, respectively. In contrast, to form full coverage, the controls samples were grown for 7 hours.

Raman spectroscopy and SEM techniques were used to characterise the uncoated and diamond coated samples.

## 2.1.3 Polymer Coating bSi

The samples were washed in absolute ethanol to remove any pre-existing bacteria and dried with a stream of compressed air. The samples were then submerged in 2 mL of an aqueous solution of polyDADMAC (0.4  $\mu\text{L}/\text{mL}$ ) for 20 mins. Excess polymer was washed away by

immersing the samples for 3 mins in aqueous NaCl (0.15 M) which was repeated two more times followed by deionised water for 30 mins to remove any excess ions and then left to air dry in sterile conditions.

X-ray photoelectron spectroscopy (XPS) was used to confirm the attachment of the polyDADMAC to the surface.

## 2.2 Determining Surface Energy

Using the Zisman plot method, the surface energies were calculated for the diamond coated and uncoated flat silicon samples. [49]

Each sample was washed in ethanol, methanol, acetone and deionised water prior to the experiment. 1  $\mu$ L drops of aqueous acetic acid at varying concentrations (2.5%, 5%, 10%, 30% and 50%) were placed on the surface and the Young's contact angle was measured using a contact angle goniometer.

## 2.3 Antibacterial Surface Testing

All solutions were sterilised using an autoclave before use.

### 2.3.1 Bacterial Culture Preparation

#### 2.3.1.1 *E. coli*

The University of Bristol Oral and Dental School supplied the *E. coli* K12 bacteria used in this study. Prior to each experiment 37.5  $\mu$ L of bacteria were inoculated into 15 mL of Tryptic Soy Broth (TSB, Oxoid) and left to grow for 16 hours in aerobic conditions at 37 °C in a shaker incubator set at 220 rpm. The bacterial suspension was then diluted into TSB to an optical density measured at a wavelength of 600 nm ( $OD_{600}$ ) 0.1 and further incubated until mid-exponential phase was reached. Bacterial cells were then harvested by centrifugation (7 mins, 5000 g), washed twice in 10 mM tris-HCl buffer, and suspended in tris-HCl to  $OD_{600}$  0.3 (approximately  $10^7$  cfu ml<sup>-1</sup>)

Each sample was washed in absolute-ethanol, air dried prior to bacterial adhesion experiments and placed in a 12-well microtiter plate. The samples were submerged in 2 mL of *E. coli* suspension and incubated for 1 hr at 37 °C under static aerobic conditions. The samples were then rinsed three times with tris-HCl buffer in a uniform manner (pH 7, Sigma Aldrich) to remove any non-adherent bacteria.

1 mL of a solution of 3  $\mu$ L/ml of Live/Dead® BacLight™ in tris-HCl buffer was added to each sample surface and incubated in the dark at 21 °C for 15 mins and finally rinsed using tris-HCl

buffer. Bacterial cell viability was then visualised by fluorescence microscopy. IMAGEJ software was used to calculate the number of cells with intact membranes (SYTO9, green) and the number of cells with damaged membranes (propidium iodide, red) based on three images per surface. The average percentage of damaged cells was determined and all tests were carried out in triplicate. A two-tailed homoscedastic Student's t-test was performed to compare data sets. If the  $p$  value was less than 0.05, then results were considered statistically significant.

### **2.3.1.2 *S. gordonii***

The University of Bristol Oral and Dental School supplied the *S. gordonii* [DL1] bacteria used in this study. The same procedure described in 2.3.1.1 was used except Brain Heart Yeast Neopeptone Infusion Broth (BHY, Lab M and SLS) was used instead of TSB and grown under anaerobic conditions.

### **2.3.1.3 Gram Staining**

Each culture was stained using crystal violet dye and safranin, staining gram-positive and gram-negative bacteria violet and pink, respectively, to check the purity of bacterial stocks.

### **2.3.2 Preparation for SEM**

Following the 1 hr incubation, the bacteria were fixed on to the surface by immersing them in 2.5% glutaraldehyde solution (Sigma Aldrich) in 0.1 M potassium phosphate buffer (potassium phosphate monobasic and potassium phosphate dibasic, pH 7.2, Sigma Aldrich) for 2 hours at 21 °C. The surfaces were then dehydrated by immersing them in 20 %, 40 %, 60 %, 80 %, 100% aqueous ethanol for 10 mins each, before hexamethyldisilazane for 10 mins.

The samples were air dried, mounted onto carbon stubs and sputtered with gold before being viewed under SEM.

## 3 Results

### 3.1 Surface Analysis

All the surfaces underwent various analytical techniques to confirm the success of the RIE, HFCVD and polymer coating processes.

#### 3.1.1 Uncoated bSi

All three lengths of bSi needles were visualised under SEM (Figure 3.1) to provide a clear image of the surface topography and to confirm that changing the RIE process varies the dimensions of the needles. As summarised in Table 2, there is a large difference in length of the needles, tip diameter and the number of spikes per unit area of the sample.

Dimension	Long Needled bSi	Intermediate Needled bSi	Short Needled bSi
Length of Needles / $\mu\text{m}$	20	2.5	0.5
Tip diameter / $\mu\text{m}$	<0.05	0.15	<0.03
Spike Density / $\mu\text{m}^{-2}$	1.5	7.8	65.2

Table 2. By varying the RIE process the dimensions of the bSi can be altered

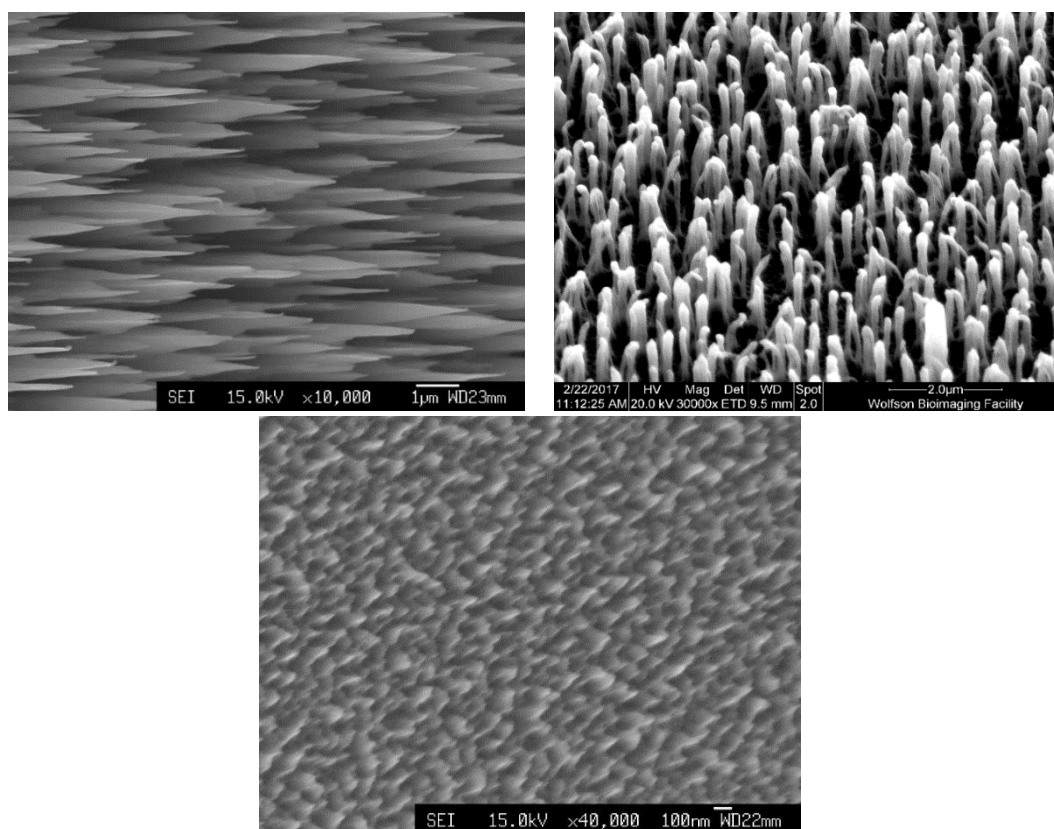


Figure 3.1. SEM images of (a) long [34] (b) intermediate and (c) short needled bSi

### 3.1.1.1 Diamond Coated Long Needled bSi

Each of the diamond coated samples underwent SEM and Raman spectroscopy to confirm a uniform coating over the nanostructures and the quality of the diamond coating on the surface.

The SEM micrographs in Figure 3.2 also provide evidence that the long needles have been uniformly coated in micro-crystalline diamond. As a consequence of this process, the needles become much thicker with a tip diameter of  $0.27\ \mu\text{m}$  compared to  $<0.05\ \mu\text{m}$  tip diameter of the uncoated long bSi needles.

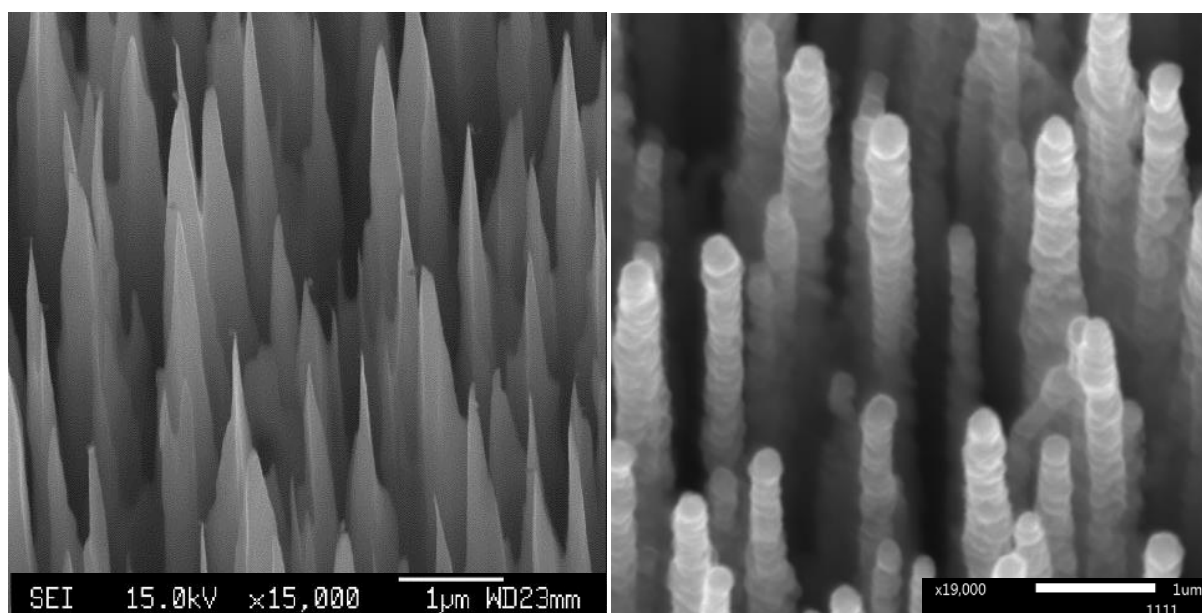


Figure 3.2. SEM micrographs of long needled bSi (a) before [34] and (b) after HFCVD process

Raman spectroscopy is a vital tool for diagnosing surface quality as different elements and even hybridisations of atoms have different characteristic peaks. Table 3 presents the characteristic peaks of silicon and diamond. [50]

Frequency / $\text{cm}^{-1}$	Assignment
520	First-order Silicon Raman peak
940	Second-order Silicon Raman Peak
1100-1150	Transpolyacetylene found at the grain boundaries
1332	First-order diamond - $\text{sp}^3$ hybridised carbon.
1345	$\text{sp}^2$ amorphous carbon
1430	Transpolyacetylene found at the grain boundaries
1520	$\text{sp}^2$ amorphous carbon

Table 3. Assignments of the characteristic Raman peaks of diamond film [50]

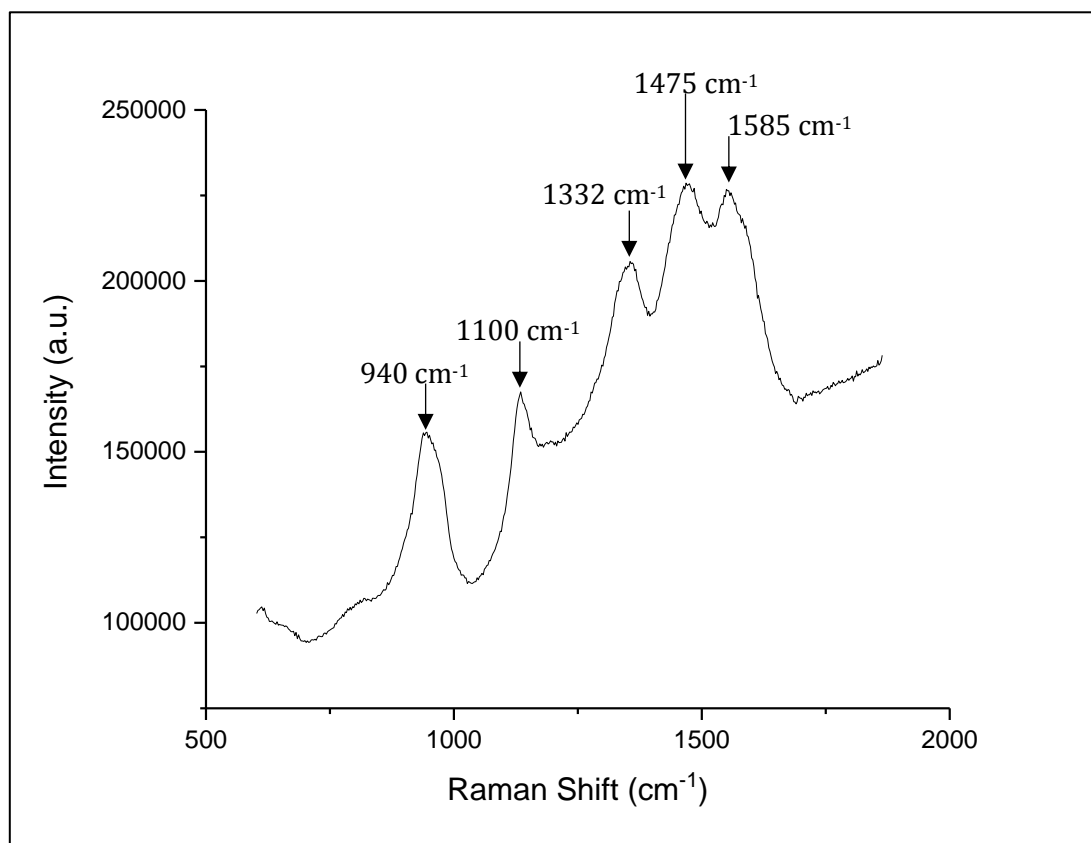


Figure 3.3. Green (514 nm) Raman spectrum confirms that the long needed bSi has been coated in diamond. The first order silicon peak at  $520 \text{ cm}^{-1}$  has been removed for clarity.

Both the SEM and Raman data provide clear evidence that the long needed bSi has been uniformly coated in diamond.

### 3.1.1.2 Diamond Coated Short Needled bSi

The HFCVD process was unsuccessful in coating the short needled bSi. The SEM micrographs, Figure 3.4, show diamond clusters forming on the surface which was confirmed by Raman spectroscopy. The lack of uniform distribution on the surface may be due to the fact that the rate of homogeneous diamond growth surpasses that of heterogeneous growth. Similar results were found when seeding the surface as described in Section 2.1.2.1. Clegg [34] also found that increasing the growth time any further would lead to the short needles being overgrown.

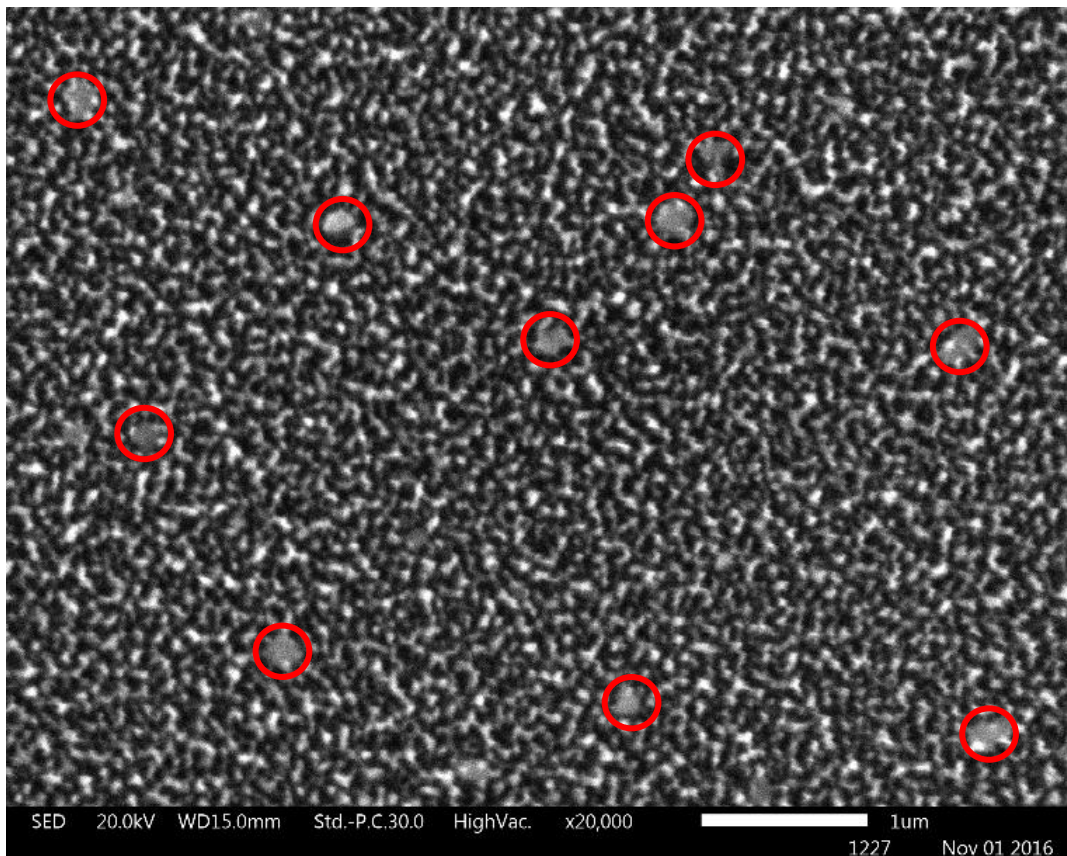


Figure 3.4. After the HFCVD process small diamond clusters can be seen on the short needled bSi

### 3.1.2 Polymer Coated bSi

XPS data and analysis was supplied by Dr Gavin Hazell. The spectra were used to confirm the presence of polyDADMAC and quaternary ammonium ions on the long needed bSi surface shown in Figure 3.5 and Figure 3.6.

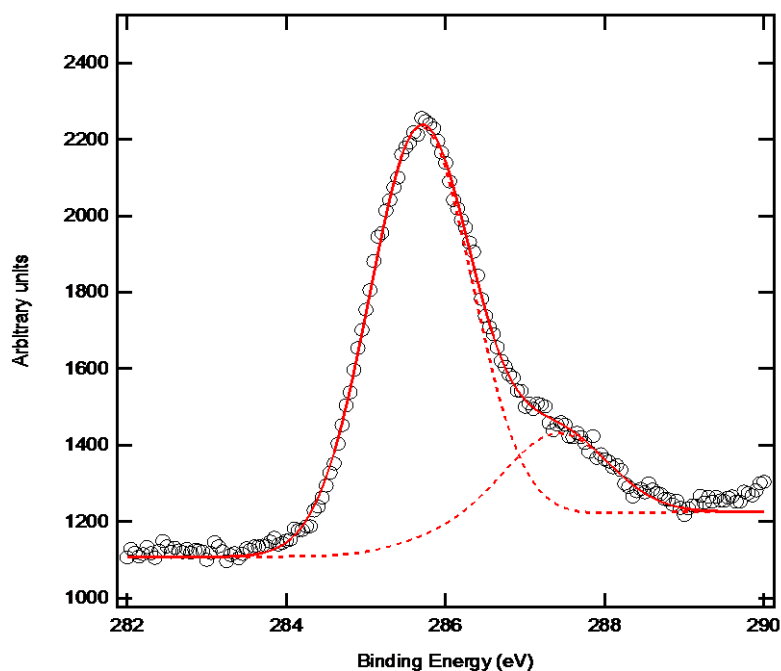


Figure 3.5. The curve-fitting deconvolution of the C1s spectra for uncoated bSi. Markers show the experimental points, dashed lines (red) the fitting components and continuous line (red) the calculated spectrum.

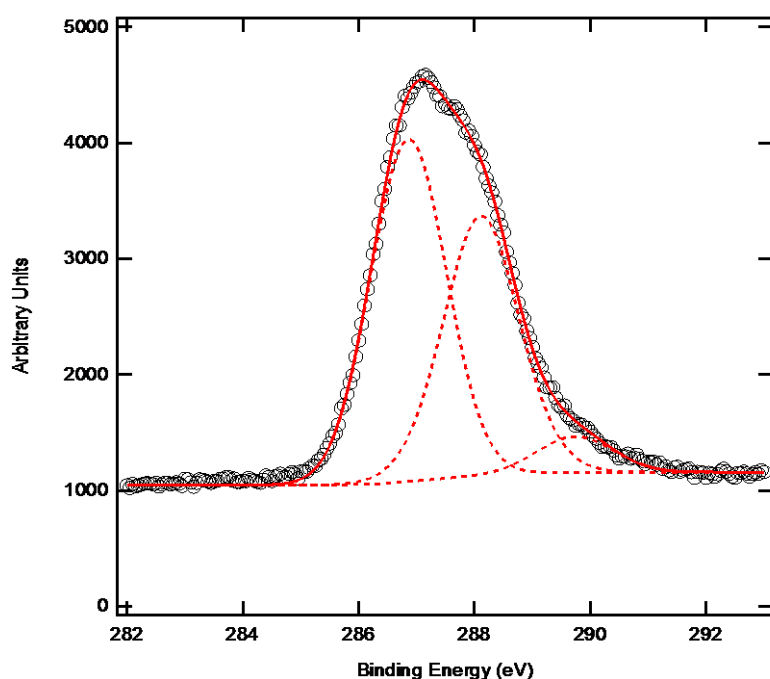


Figure 3.6. Curve-fitting deconvolution of the C1s spectra bSi functionalised with polyDADMAC. Markers show the experimental points,

A weak carbon contamination peak was found on the uncoated bSi surface, Figure 3.5, due to various chemical species (C-C, C-O) and have been denoted, in Table 4, as C1-C2. The C1s peaks change dramatically upon the adsorption of polyDADMAC to the surface shown in Figure 3.6. Here the carbon present on the surface is dominated by a peak at 286.3 eV representing the carbon bonded to a quaternary ammonium ion (C-N<sup>+</sup>).

	Signal	Component	Assignment and contribution to signal (%)
bSi	C1	C-C	285.5 (83.2)
	C2	C-O	287.4 (16.8)
bSi + polyDADMAC	<b>C1</b>	<b>C-N<sup>+</sup></b>	<b>286.3 (53.3)</b>
	C2	C-O	288.1 (41)
	C3	O-C=O	289.7 (5.6)

Table 4. Summary of XPS results and peak assignments for bare bSi uncoated and polymer coated

### 3.1.3 Surface Energy

The adhesion of bacteria onto a surface is determined by a number of factors the main contribution being the wettability of the surface. A low surface energy (high wettability) would increase the magnitude of the interaction between polar cell walls and the surface. The surface energy can be determined by measuring the contact angle using a goniometer, Figure 3.7, and Young's equation (1) where  $\theta_Y$  is the Young's contact angle,  $\gamma_{SV}$ ,  $\gamma_{LV}$  and  $\gamma_{SL}$  is the surface energy between the solid and vapour, the liquid and vapour and the solid and liquid, respectively.

$$\cos\theta_Y = \frac{\gamma_{SV} - \gamma_{SL}}{\gamma_{LV}} \quad (1)$$

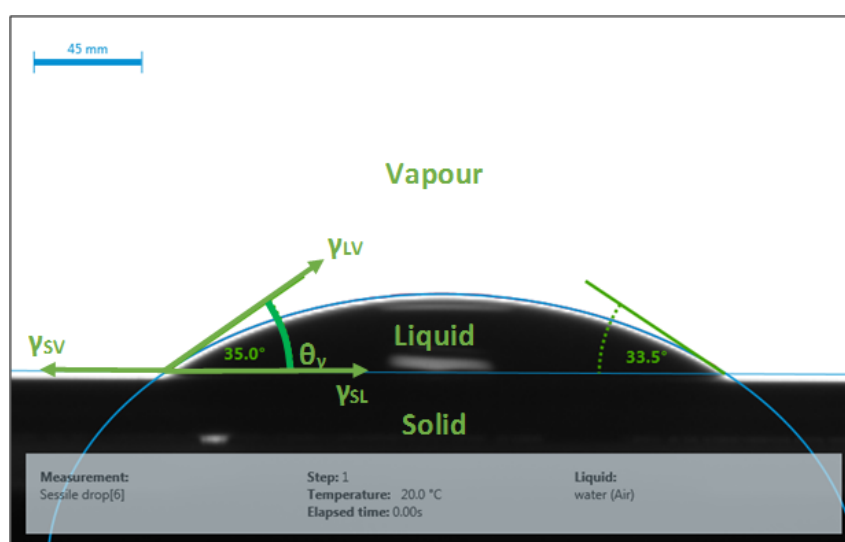


Figure 3.7. The contact angle,  $\theta_Y$ , of a sessile drop can be measured using a goniometer

The roughness of the bSi surfaces meant that any droplets on the surface immediately dispersed in between the needles before a contact angle could be measured [51]. A diamond coated flat silicon control and an n-doped silicon wafer have the same surface composition as the bSi samples and so were used instead to determine the surface energy.

The surface energies were established by Zisman's method [49]. By measuring the contact angles of solutions with differing surface tensions (i.e. varying concentrations of acetic acid) a linear Zisman plot can be produced, Figure 3.8.

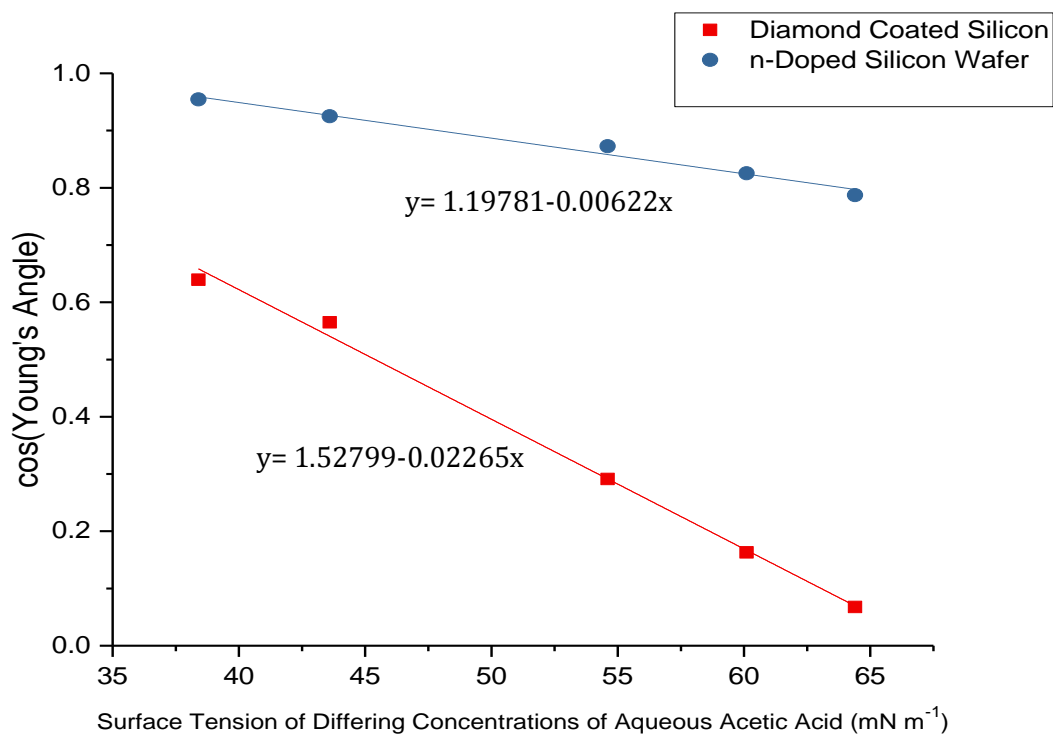


Figure 3.8. Zisman's plot of n-doped single crystal (100) silicon wafer and a diamond coated silicon wafer

By extrapolating the above plot to  $\cos\theta_{\gamma} = 1$  the critical surface tensions,  $\gamma_c$ , were calculated.  $\gamma_c^{\text{Diamond}} = 23.4 \pm 0.0437 \text{ mN m}^{-1}$  [lit.  $23.15 \text{ mN m}^{-1}$  [52]] and  $\gamma_c^{\text{Silicon}} = 31.9 \pm 0.0258 \text{ mN m}^{-1}$  [lit. =  $42.7 \text{ mN m}^{-1}$  [53]].

Variations from the literature may be due to the surface chemistry, such as the addition of dopants, or the surface topography of the polycrystalline diamond [54], [55]. The large difference between the literature and experimental value for the silicon wafer may be due to variations of the extent of oxidation of the surface. Nevertheless there is a clear result that the wettability of the diamond coated control is much higher than that of n-doped silicon wafer.

### 3.2 Live/Dead Assay

The gram staining confirmed the purity of each stock as any gram-negative or gram-positive bacteria that are contaminants will be pink or violet for, respectively, as shown in Figure 3.9.

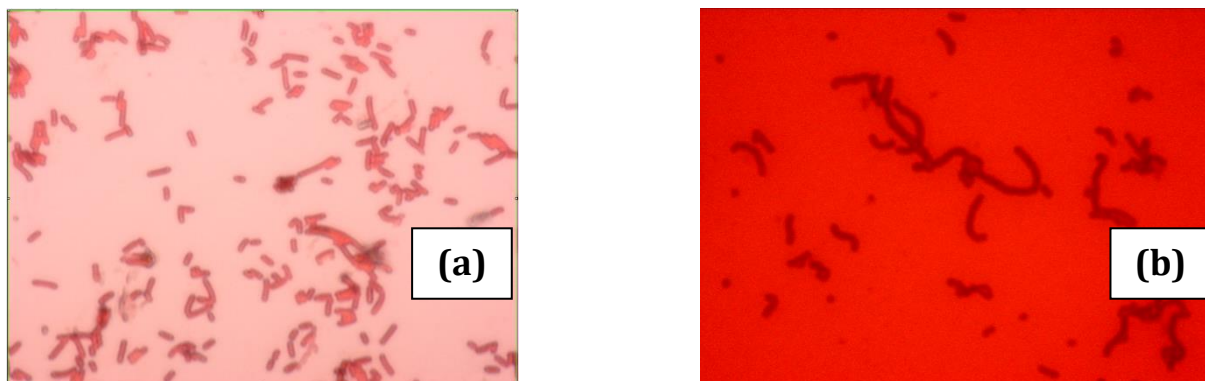


Figure 3.9. Gram-stain images (a) gram-negative bacteria, *E. coli*, has been stain pink and (b) gram-positive bacteria, *S. gordonii*, has been stained violet.

The kill ratio of motile, gram-negative bacteria, such as *E. coli*, produced the most successful results on nanostructured surfaces, as described in section 1.6. Therefore to confirm the bSi needles had bactericidal effects, *E. coli* was tested first. After incubation, the Live/Dead BacLight® dyes were added to the surface which resulted in the live and dead cells fluorescing green and red respectively in fluorescence microscopy, as shown in Figure 3.10. The cells were then manually counted using the software IMAGEJ to determine the live/dead ratio and the total cellular adhesion to the surface. Each of the measurements were analysed using the two-tailed Student's t-test. Significance values are listed as  $p < 0.05$  (\*),  $p < 0.01$  (\*\*),  $p < 0.001$  (\*\*\*),  $p < 0.0001$  (\*\*\*\*).

### 3.2.1 Uncoated bSi

The first area of interest was to determine how the bactericidal nature of a surface is affected by the topography by varying the height, sharpness and spike density of the nanostructures. This was carried out using short, intermediate and long needled uncoated bSi. Representative fluorescence micrographs of these three surfaces, in addition to the flat silicon control, are shown in Figure 3.10.

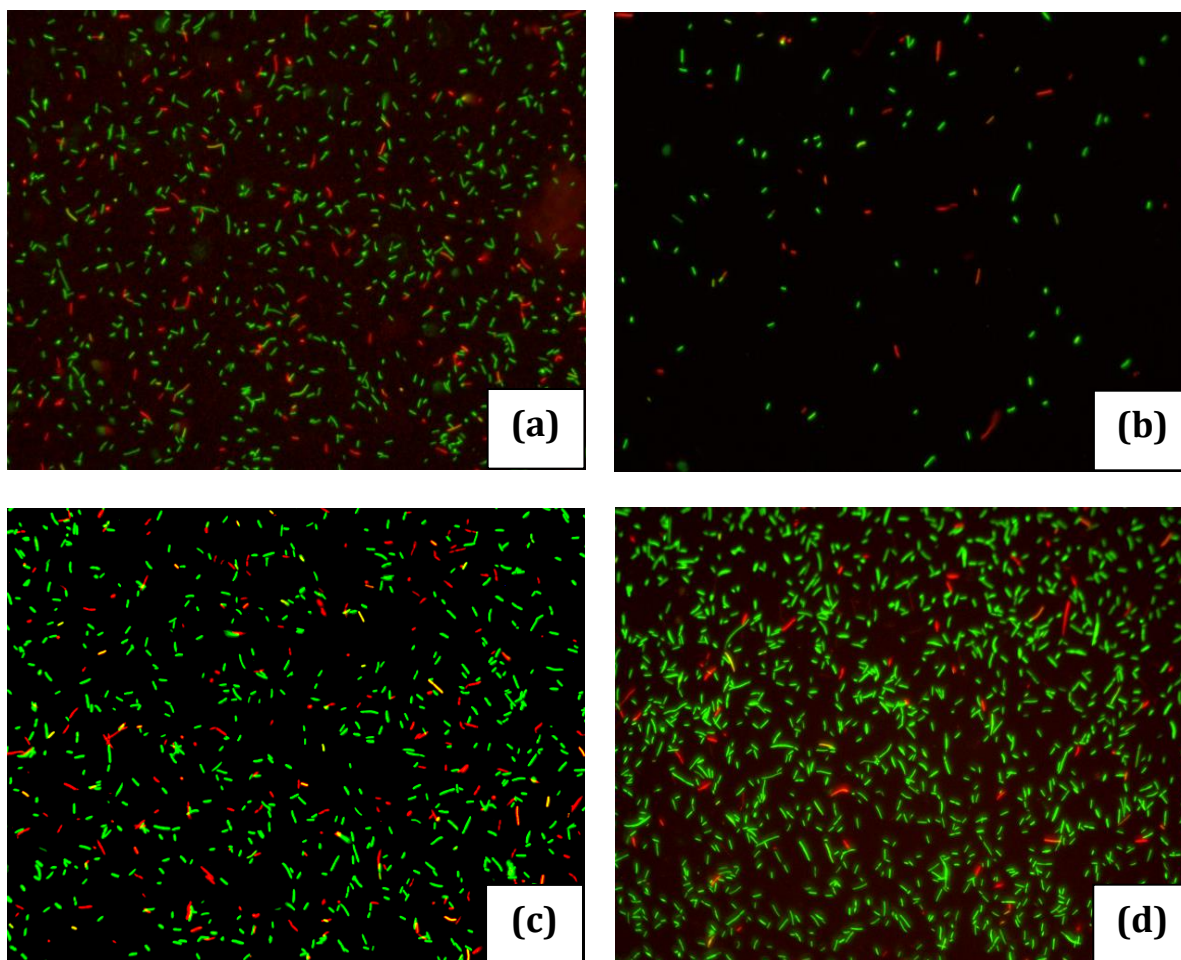


Figure 3.10. Fluorescence micrographs of *E. coli* after 1 h incubation on (a) long needled (b) intermediate needled and (c) short needled bSi and (d) flat Si controls at  $\times 20$  magnification

The cell live/dead ratio was counted as shown Figure 3.11. All the nanostructured surfaces increase the cell death ratio from 6% to 23%, 30% and 31% for long, intermediate and short needed bSi, respectively. All nanostructures are have a significant value  $p < 0.0001$  compared to the flat Si controls.

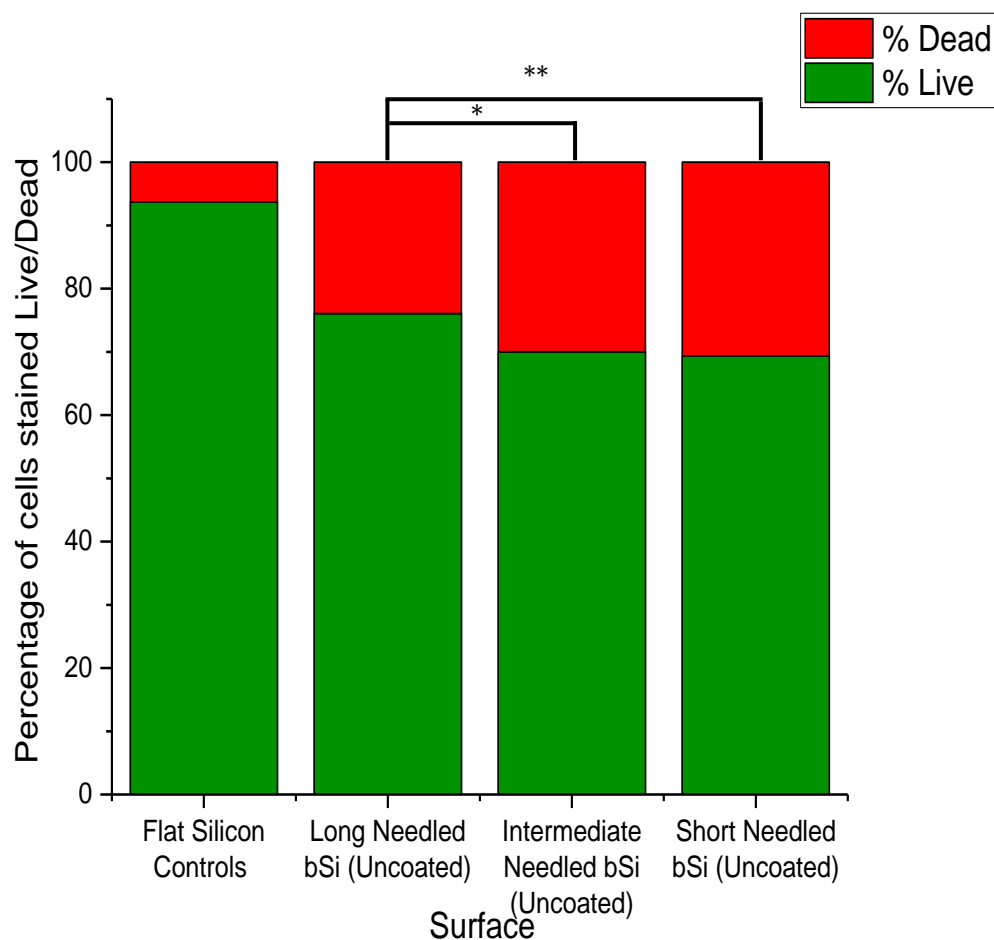


Figure 3.11. The percentage of *E. coli* cells stained live/dead on the flat silicon controls and the long, intermediate, and short needed bSi

The total number of cells adhered to the surface were counted, the highest adhesion was found on the flat silicon controls with 1805 compared to 779, 133 and 603 for the long, intermediate and short needled bSi as shown in Figure 3.12.

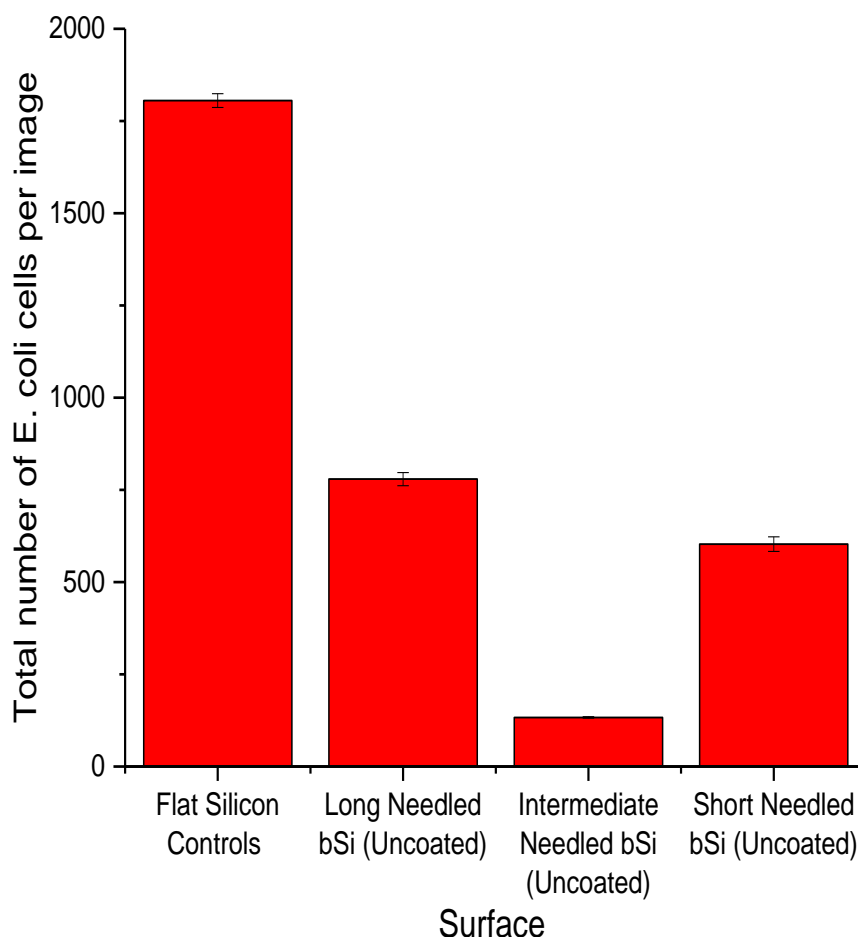


Figure 3.12. Total average number of adhered *E. coli* cells per image on the flat silicon controls and the long, intermediate and short needled bSi surfaces

### 3.2.2 Diamond Coated bSi

The diamond coated long needled bSi samples were not as effective at killing bacteria than the uncoated long needled bSi, as demonstrated in Figure 3.13 and Figure 3.14, with a cell death of only 20% and 23%, respectively. Furthermore, the diamond coated needles do not have a significant value ( $p < 0.05$ ) when analysed against both the diamond coated control or the uncoated bSi. In consequence, there is no conclusive evidence that the diamond coated needled bSi are increasing the kill ratio compared to the flat diamond coated controls.

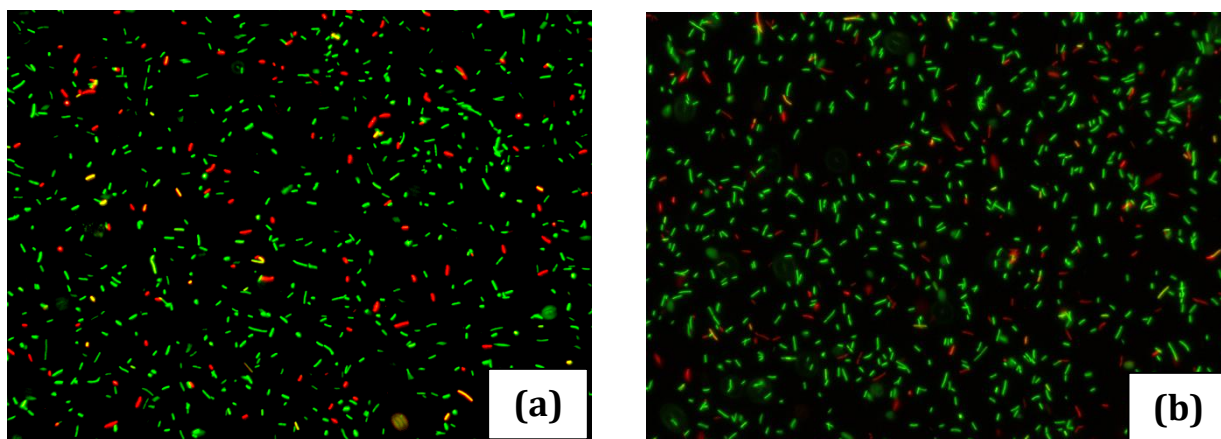


Figure 3.13. Fluorescence micrographs of *E. coli* after 1 h incubation on (a) diamond coated long needled bSi and (b) flat diamond control at  $\times 20$  magnification

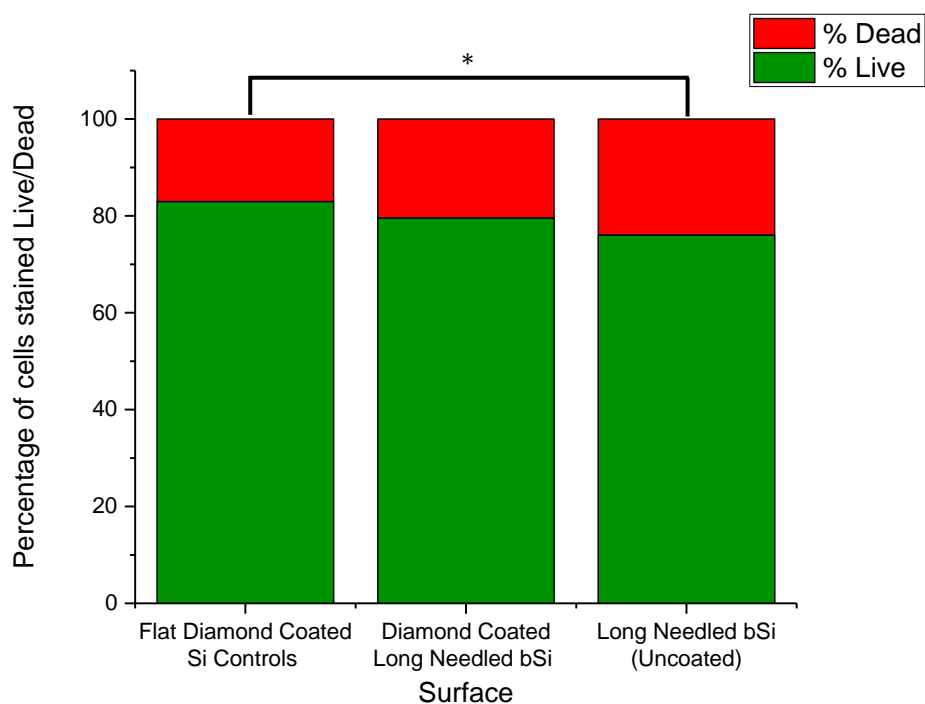


Figure 3.14. The percentage of *E. coli* cells stained live/dead on the diamond coated long needled bSi compared to uncoated long needled bSi and a flat diamond control

On the other hand, the total average adhesion to the diamond coated bSi needles is by far the highest compared to the uncoated long needled bSi, with a total average of 1011 and 779 adhered cells, respectively, as shown in Figure 3.15.

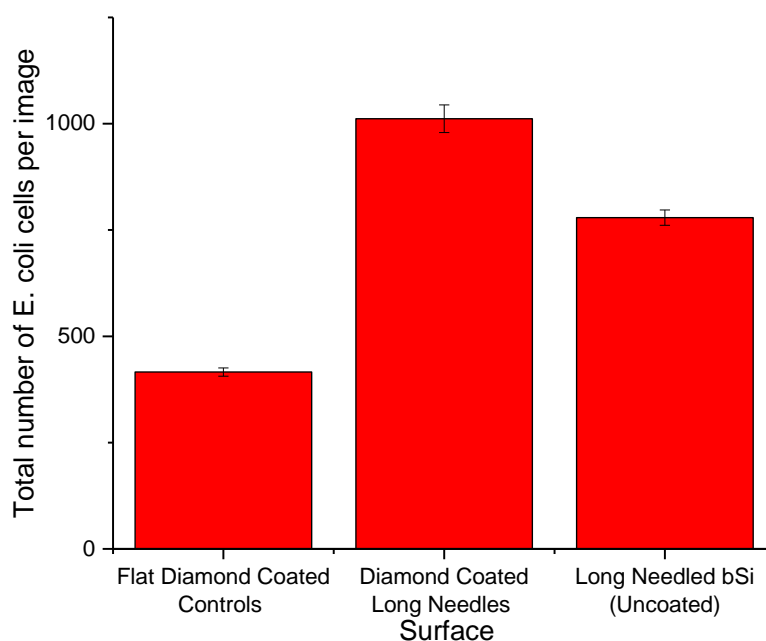


Figure 3.15. Total average number of adhered *E. coli* cells per image on the diamond coated bSi compared to uncoated long needled bSi and a flat diamond control

### 3.2.3 Polymer Coated bSi

The processes were repeated for the polymer coated surfaces producing Figure 3.16 and Figure 3.17.

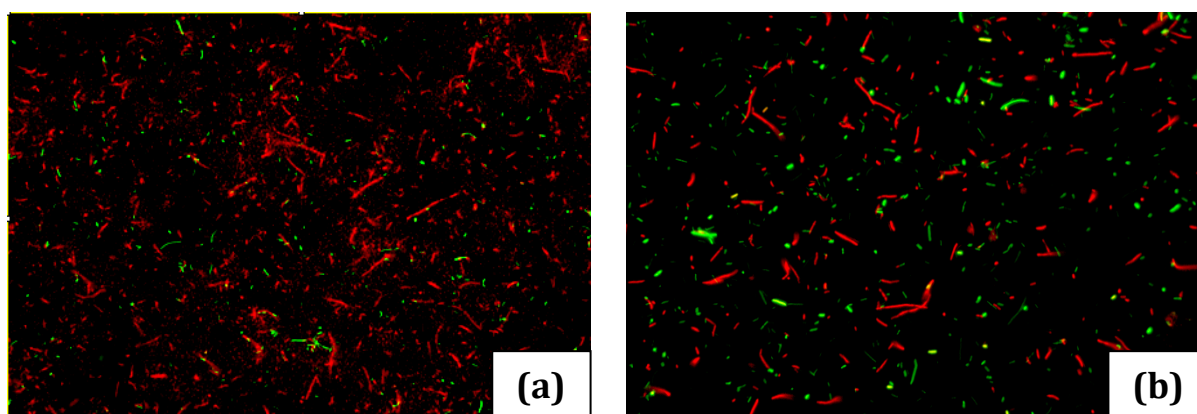


Figure 3.16. Fluorescence micrographs of *E. coli* after 1 h incubation on (a) polymer coated long needled bSi and (b) polymer coated flat Si control at  $\times 20$  magnification

An increase in cell death from 37 % to 54 % (Figure 3.17) with the addition of the nanostructures coupled with elongation of some *E.coli* cells (shown in Figure 3.16 (a) and (b)), discussed later, means that a chemical and physical mechanism for killing the bacteria can be inferred.

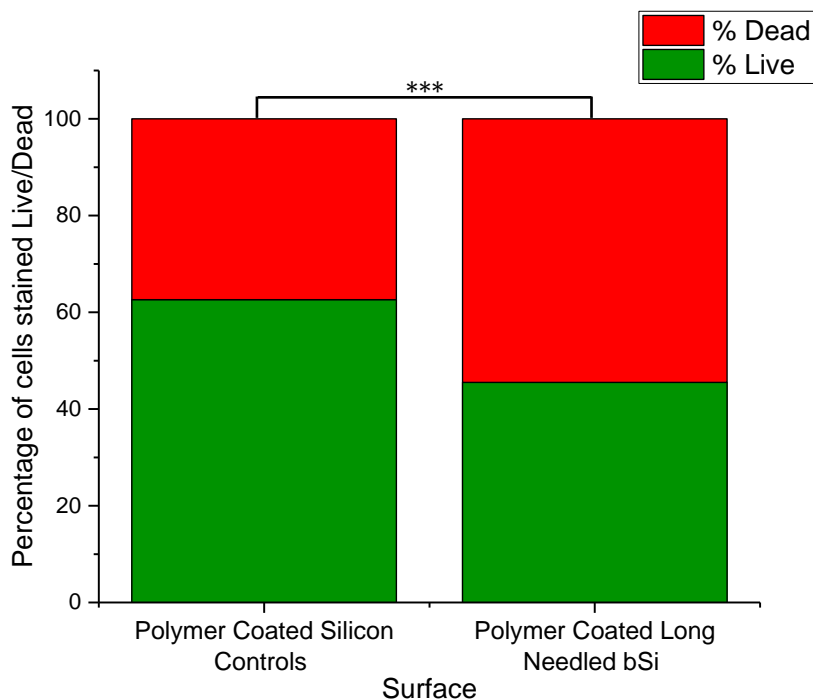


Figure 3.17. The percentage of *E. coli* cells stained live/dead on the polymer coated long needed bSi and polymer coated flat Si control.

The polymer coating did not have the desired effect on adhesion, which actually decreased with the addition of the polymer from 779 on the uncoated long needed bSi sample to 640 adhered cells, as shown in Figure 3.18.

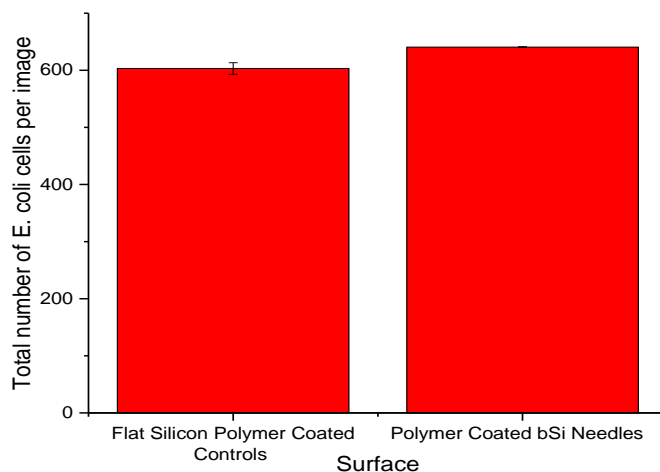


Figure 3.18. Total average number of adhered *E. coli* cells per image on the polymer coated Si controls and long needed bSi

### 3.2.4 *S. gordonii*

The short needles exhibited the highest cell death (with a purely physical kill mechanism not found on the polymer surfaces), and so the effectiveness of this surface was tested further with a gram-positive, non-motile bacteria, *S. gordonii*. However, there was only an increase in cell death of 0.23 % upon the addition of the nanostructures, as shown in Figure 3.20 and Figure 3.19. Furthermore, the data obtained does not pass the student t-test, therefore there is insufficient evidence to confirm the short needled bSi have any bactericidal properties towards *S. gordonii*.

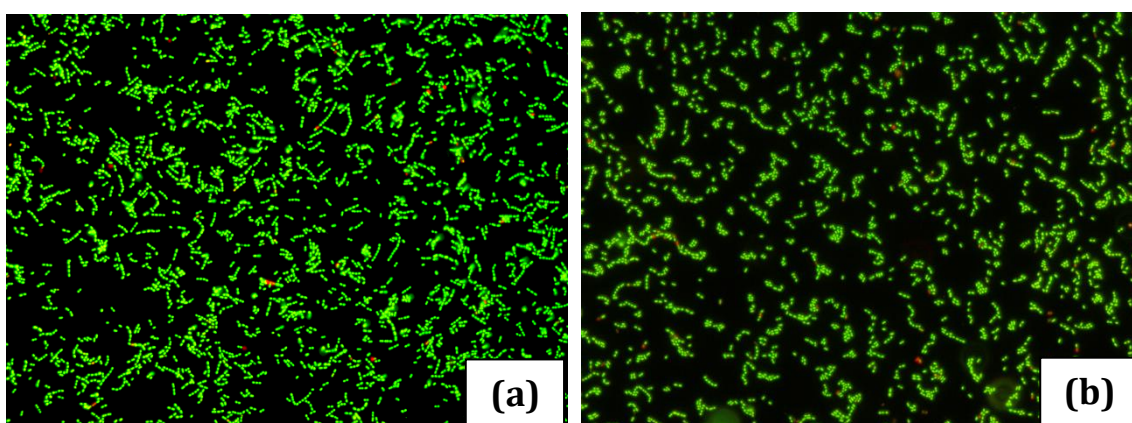


Figure 3.20. Fluorescence micrographs of *S. gordonii* after 1 h incubation on (a) short needled bSi and (b) flat Si control at  $\times 40$  magnification

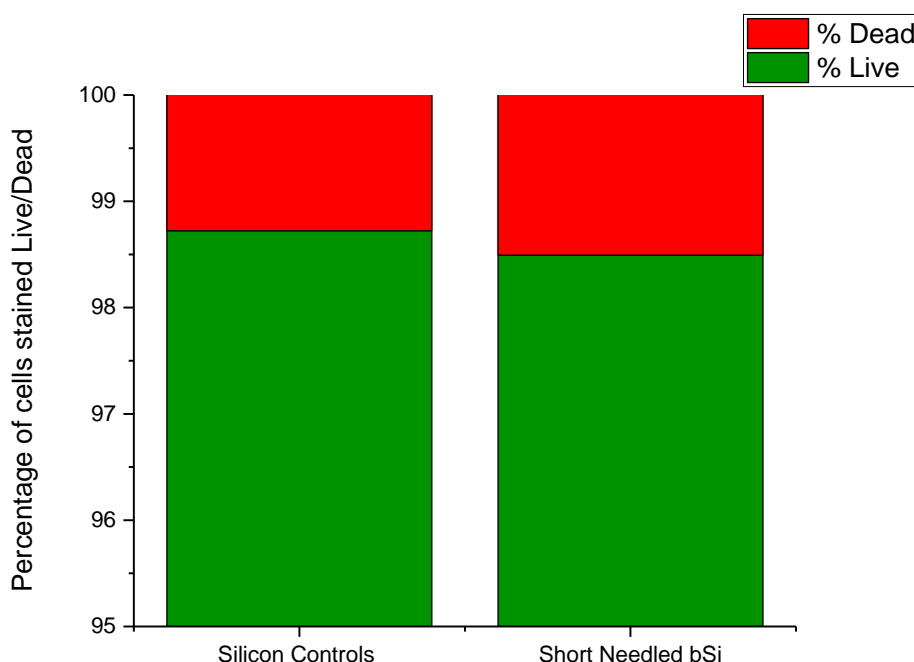


Figure 3.19. The percentage of *S. gordonii* cells stained live/dead on flat Si controls and the short needled bSi

## 4 Discussion

---

### 4.1 Live/Dead Assays

Cellular and membrane integrity is the main criterion to determine the viability of a bacterial cell. Live (viable) cells have an intact, tight membrane whereas dead cells are thought to have a disrupted cell membrane causing it to be more permeable.

Live/Dead BacLight® contain the two fluorophores; SYTO9 and propidium iodide (PI). SYTO9 is able to enter both live and dead cells and the green fluorescence is enhanced upon intercalation with DNA. PI, however, can only penetrate the disrupted cell membranes of dead cells. Once inside PI can displace SYTO9 due to its higher binding affinity to DNA,  $3.9 \times 10^5/\text{M}$  and  $1.8 \times 10^5/\text{M}$  respectively, resulting in an enhanced red fluorescence for dead cells.

However, in practice this is not always the case, for a number of reasons. Cells may be metabolically inactive yet still have a fully intact membrane which cannot be penetrated by PI. Contrary to this, during the exponential growth in a nutrient-rich environment, the membrane integrity of cells are reduced allowing PI to enter viable cells. Viable cells may even expel SYTO9 from the cytoplasm and will not fluoresce at all, and in some cases PI does not fully displace SYTO9 resulting in a yellow fluorescence; these cells are classed as dead. However, these scenarios are rare and will occur equally on all surfaces so results from the live/dead assay can be deemed reliable when comparing them to one another. [56]

### 4.2 Physical Killing Mechanism

The SEM micrographs confirm that the needles disturb the cell wall of *E. coli*, but to varying degrees depending on the taper of the needle. As can be seen in Figure 4.1 (a), the longer needles, with a longer taper and thinner tip, are able to completely spear the bacteria. In contrast, the short and intermediate needles are less aggressive in puncturing the cell wall, but are still effective as shown in Figure 4.1 (b), causing the intercellular contents to leak out.

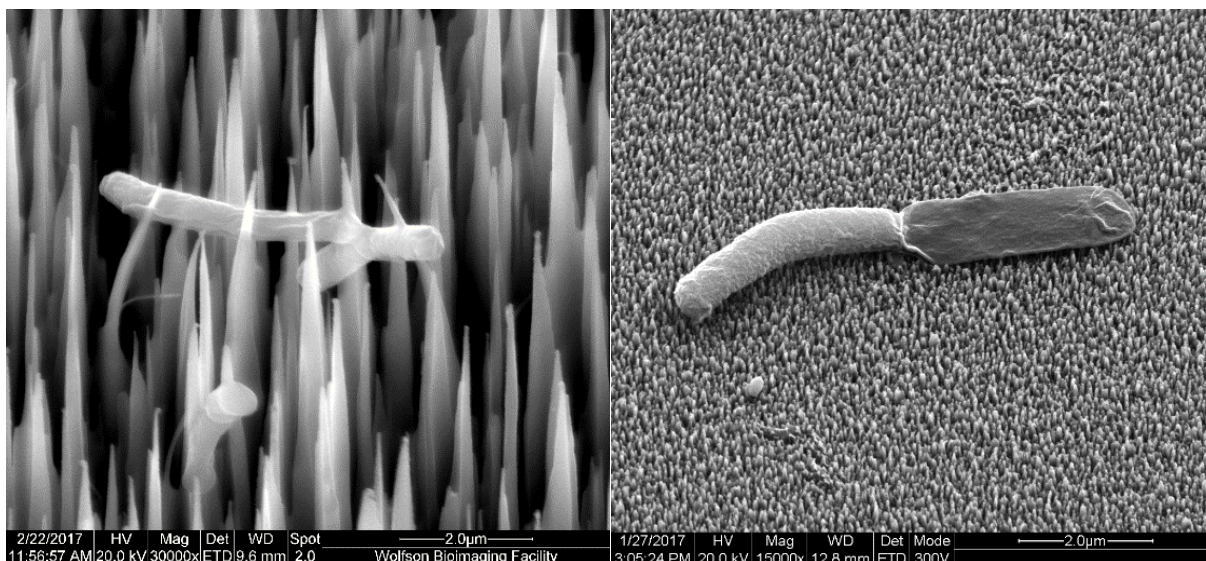


Figure 4.1. *E.coli* cell wall is ruptured by both (a) (polymer coated) long needled bSi and (b) short needled bSi.

The disruption of the membrane primarily starts as an indentation in the cell wall which is demonstrated in Figure 4.2, where the bacteria have been fixed during this indentation process and have detached from the nanostructures leaving the imprint visible.

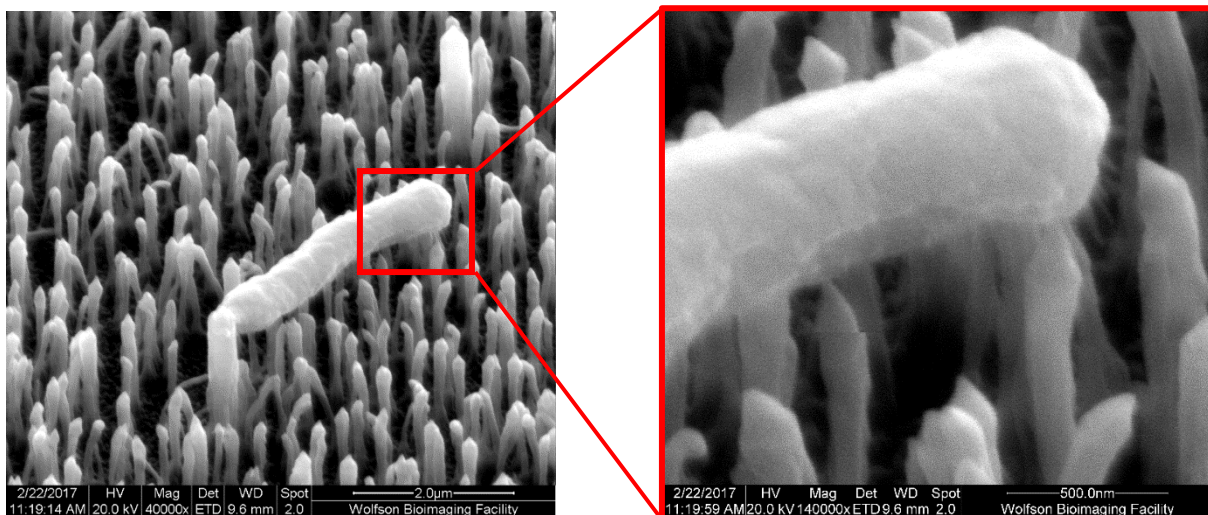


Figure 4.2. *E.coli* on intermediate bSi needles

However, there is a lack of evidence suggesting that the taper of the needles has an effect on the bactericidal nature, because even though the long needles are able to spear the bacteria, both the short and intermediate needles have a cell death ratio ~6% higher than the long needles.

As an aside, it was commonly found on the long needled bSi (uncoated and polymer coated) that once a cell adheres to the surface the motile *E. coli* bacteria tend to spread out in a 'tip-toe' fashion (section 1.5.2), in an attempt to disperse their weight across many needles and find a smoother area on the surface, but in doing so stretches so far that the membrane ends up rupturing.

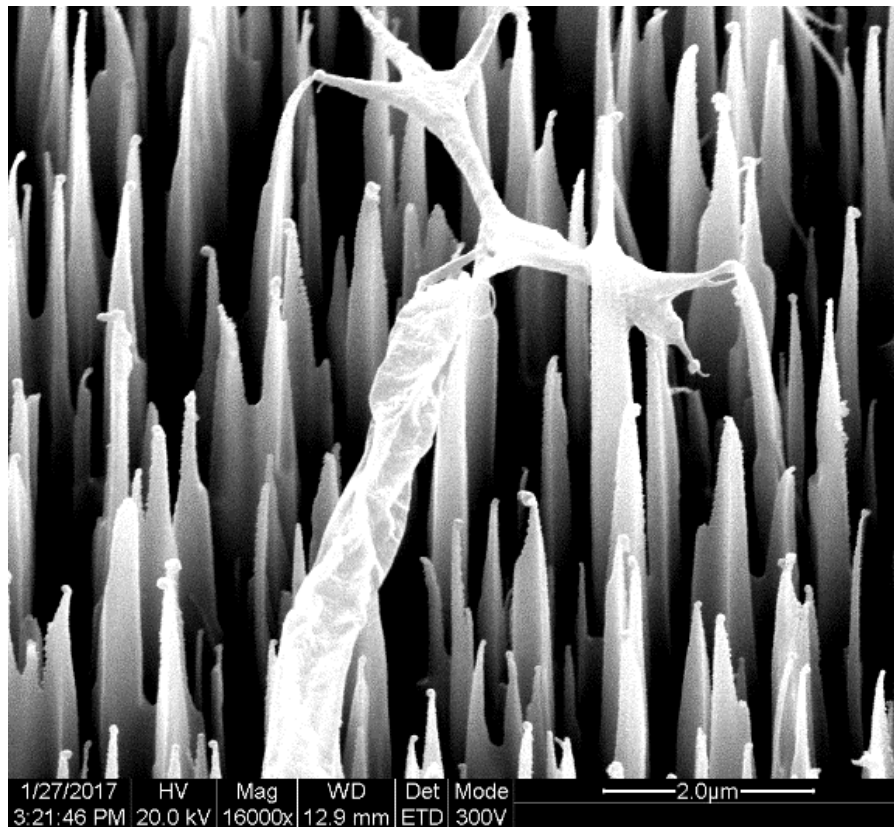


Figure 4.3. In an attempt to find a smoother area of the surface the *E. coli* bacteria spread out.

## **4.3 The Relationship between Surface Topography/Chemistry and Cell Death Percentage**

### **4.3.1 Adhesion**

In section 1.5.2, it was hypothesised that increasing the adhesion of bacteria to the surface would lead to a stronger pulling force of the bacteria onto the needles leading to an increase in the cell death percentage. However, the results above contradict this statement.

The diamond coated long needled bSi have the highest total adhesion number with an average of 1011 cells compared to any of the uncoated bSi needles. This may be due to the wettability of the diamond surface, as calculated in section 3.1.3, being much higher than that of an n-doped silicon wafer. Despite this, the diamond coated needled bSi have the lowest cell death, only being 20%.

The intermediate needles have by far the lowest adhesion rates, being only 133 cells and yet the second highest cell death percentage at 30%. This low adhesion may be due to similar reasons to those which allow shark skin to be self-cleaning as described in section 1.4. Even though the dimensions of the needles are an order of magnitude larger than the grooves on shark skin, they may still prevent the attachment of the bacteria onto the nanostructures in a similar manner.

### **4.3.2 Tip Diameter**

It has been established that when comparing the diamond coated and uncoated long needled bSi, the differences in surface chemistry between diamond and n-doped silicon, does not have an effect on the cell death ratio. It can therefore be assumed the main variable when comparing these two surfaces is the difference in tip diameters of 0.27  $\mu\text{m}$  (diamond coated) and <0.05  $\mu\text{m}$  (uncoated). This increase in tip diameter may account for the detrimental effect of the bactericidal nature of the surface from a cell death percentage of 24% to only 20% upon diamond coating the surface.

The intention of diamond coating the bSi was to increase the resilience of the needles, which may be scratched off. However, since the diamond coating is so thin there is a negligible increase of resilience. Coupled with the detrimental effect to the bactericidal nature, as well as the fact that bSi is already biocompatible, no more work was done towards finding a way to uniformly diamond coat the short and intermediate needles.

### 4.3.3 Spike Density

As mentioned before in Table 2 the long needled bSi has a much lower spike density of  $1.5 \text{ spikes } \mu\text{m}^{-2}$  than that of both the intermediate and short needled bSi,  $7.8 \text{ spikes } \mu\text{m}^{-2}$  and  $65.2 \text{ spikes } \mu\text{m}^{-2}$ , respectively. This leads to the bacteria fitting in between the needles rather than sitting on top of the needles, as shown in Figure 4.4. This may account for fewer bacteria being pierced and dying even though the adhesion number is so much higher than that of the short and intermediate needles.

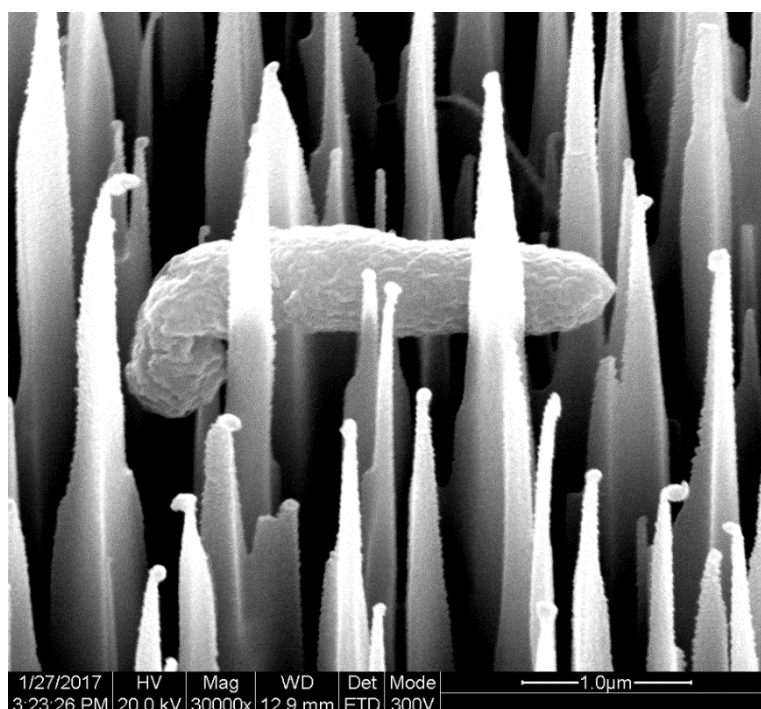


Figure 4.4. An *E.coli* cell can fit in between the long bSi needles and prevent the cell wall being ruptured by the needles.

Even though there is a large difference in spike densities between the short and intermediate needles the kill percentage is very similar. This may suggest there may be an optimum spike density where once reached, the kill rate may plateau or even decrease suggesting a 'bed-of-nails' regime [57]. This theory can be supported by the stretching theory model in 1.5.1. As the needles become more closely packed, the  $S_B$  decreases which in turn governs the stretching threshold, leading to an increase in the force needed to surpass it.

#### 4.3.4 Polymer Coating

The polymer did not have the desired effect of increasing adhesion, but as mentioned before there is no evidence suggesting that the kill percentage is a function of total adhesion.

From Figure 3.16 (a) and (b) it is clear that both the polymer coated controls and bSi have dead elongated *E. coli* cells. This suggests that there is both a physical and chemical synergic killing mechanism. There are two possible causes of this elongation, residual NaCl left from the washing process or the polyDADMAC polymer.

First, studies conducted by Hajmeer *et al.* [58] found that *E. coli* elongate under salty conditions with NaCl concentrations exceeding 8%. These irregularities in cell morphology are from the partial disruption of the peptidoglycons, cytoplasm and cytoplasmic material. Residual salt left behind from the washing process of the sample may be the cause for these observed elongations.

Alternatively, the more likely cause for these deaths may be the fact that polyDADMAC has a high concentration of quaternary ammonium centres which has been found to have bactericidal effects against gram-positive, gram-negative and multidrug resistant bacteria.

With the long alkyl chains and the polar centre polyDADMAC acts as an amphiphilic molecule with the cationic ammonium head group and a hydrophobic alkyl tail. The cationic head group interacts with the anionic phosphate heads found in the phospholipid bilayer while the alkyl tails lodge themselves in the hydrophobic core of the membrane as shown in Figure 4.5 . The phospholipids become dislodged causing a decrease in membrane fluidity and the creation of hydrophobic voids in the membrane. Protein function is perturbed which leads to the disintegration of the cell and solubilisation of proteins and phospholipids into quaternary ammonium compounds and phospholipid micelles. But there is no evidence of this causing elongation of the cell. [59], [60]

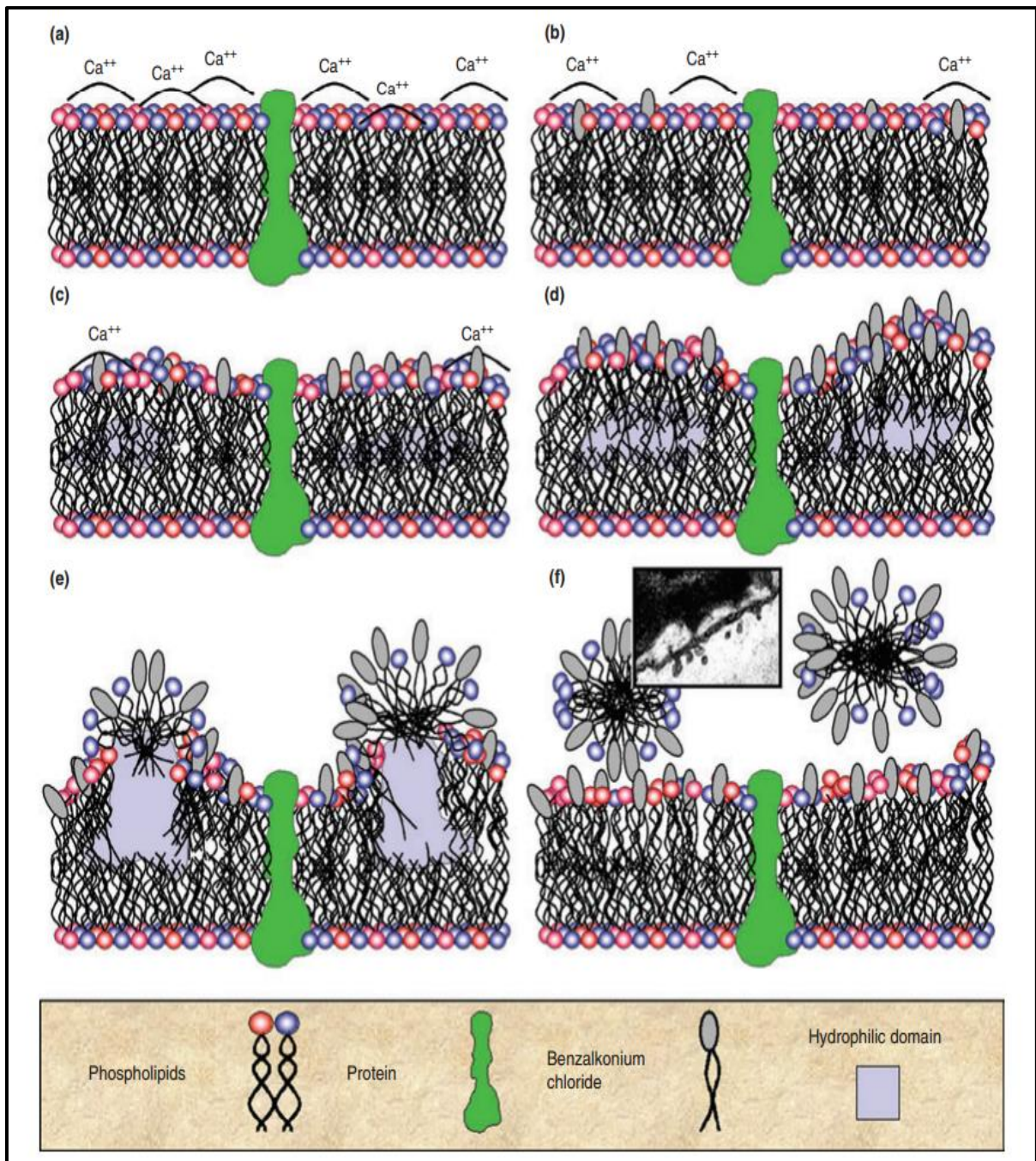


Figure 4.5. Schematic diagram demonstrating the mechanism by which quaternary ammonium compounds (i.e. polyDADMAC or benzalkonium chloride) act as surfactants, lodging themselves into the bilayer of the cell membrane. In doing so the membrane fluidity decreases and hydrophilic voids form within the membrane. These voids eventually become micelles which are expelled from the cell membrane. Inset: a micrograph showing vesicle formation. [59]

#### 4.3.5 *E. coli* versus *S. gordonii*

The short needled bSi samples were much less successful at killing *S. gordonii* [DL1] than *E. coli* [K12]. This may be down to two reasons. Firstly, *E. coli* is a gram-negative bacteria. As discussed in section 1.5, the thin membrane is very elasticated and is penetrated more easily by nanostructures than the much thicker gram-positive bacterial membrane of *S. gordonii*. Alternatively, as seen in Figure 4.3 the motile *E. coli* 'tip-toe' and spread out on the surface, straining and eventually rupturing the cell wall. *S. gordonii*, in contrast, are non-motile and once attached to the surface do not move or spread out across the surface, therefore the cell wall does not undergo any extra strain resulting in fewer cells dying.

## 5 Conclusions

---

Using *E.coli* [K12] it was confirmed, by fluorescence microscopy, that bSi can be used as a bactericidal surface due to its nanotopographical features. SEM images were used to provide evidence for the physical mechanism by which the bacteria are killed, this is due to the rupturing of the cell wall as outlined by the stretching theory.

The long needled bSi surfaces were successfully coated with a diamond film *via* HFCVD. In contrast, the short needled bSi were not successfully coated in diamond. This may be due to the homogeneous growth rate surpassing that of the heterogeneous growth rate, resulting in diamond clusters found arbitrarily on the surface. Either way, evidence suggests that diamond coating the needles is, in fact, detrimental to the bactericidal nature of the nanostructure, discussed below.

The main aim of this project was to determine which characteristics of a nanostructure contributed to an increase in the cell death percentage of the bacteria. Specifically; adhesion, tip diameter, spike density, and length of needles of bSi.

### 5.1 Adhesion

Firstly, the wettability of the surface was increased by diamond coating the bSi needles *via* HFCVD, thus increasing the adhesion of *E. coli* from 779 to 1011 average total number of adhered cells. However, the increase in cell adhesion had very little effect on the cell death percentage, with a 3% decrease upon the addition of the diamond film. The intermediate length needled bSi had the lowest total adhesion of 133 cells and yet one of the highest cell death percentages, at 30%. From this it can be inferred that there is no correlation between the cell death percentage and the cell adhesion on a nanostructured surface.

### 5.2 Tip Diameter

The addition of the diamond film on the long needled bSi resulted in a large increase in tip diameter compared to the uncoated long needled bSi, from  $<0.05$  to  $0.27 \mu\text{m}$ . Since it has been established that adhesion has no effect on cell death it can therefore be assumed that the difference in cell death percentage of 20% (diamond coated) and 24% (uncoated) on the bSi surface is probably the result of the increase in tip diameter.

### 5.3 Length of Needles

Even though the SEM images show that the long needles are more effective at completely spearing the bacteria there is no evidence that this is a contributing factor since the short and intermediate needles have a much higher cell death percentage of 23%, 31% and 30%, respectively.

### 5.4 Spike Density

If the length of the needles is not a contributing factor, the main difference, especially comparing the long and short needles, is the spike density. The long needles have a very low spike density of 1.5 spikes  $\mu\text{m}^{-2}$  compared to the short needles of 65.2 spikes  $\mu\text{m}^{-2}$ . This resulted in the bacteria being able to orientate themselves in between the long needles and therefore prevented the cell wall from rupturing and causing the cells to die. The short needles, in contrast, are much more closely packed and so the bacteria are unable to fit in between the needles, and therefore will always come into contact with the tips.

There is little difference in kill percentages between the intermediate and the short needles; 30% and 31% respectively. This may mean there is an optimum spike density after which the kill percentage plateaus and may eventually decrease as the weight of bacteria is spread out so much the needles no longer have an effect.

### 5.5 PolyDADMAC

The addition of polyDADMAC did not have the desired effect of increasing adhesion to the surface. The cell adhesion of polymer coated and uncoated long needled bSi was 640 and 779 cells respectively.

In spite of this, the images from the fluorescence microscopy showed elongation of *E. coli* in both the polymer coated flat controls and the bSi needles. This may provide evidence of a synergistic chemical and physical killing mechanism. The chemical mechanism is most likely due to the quaternary ammonium group with an alkyl group attached acting as an amphiphilic molecule, which inserts and destabilises the phospholipid membrane of the cell causing it to form micelles. Alternatively it may be due to residual NaCl ions found on the surface or the Cl<sup>-</sup> ions associated with the positively charged quaternary ammonium group.

## 5.6 *S. gordonii*

The main differences to note between *E. coli* and *S. gordonii* are that they are gram-negative and motile, and gram-positive and non-motile, respectively. These differences may account for the fact that the short needled bSi had no bactericidal properties against *S. gordonii* and may be explained by two possibilities. First, the gram-positive cell wall is much thicker and may be almost impenetrable by the nanostructures compared to the much thinner, elasticated cell wall of the gram-negative bacteria. However, *S. gordonii*, is much less motile than *E. coli* and much less 'tip-toeing' was seen from these bacteria; this may mean the cell wall is put under much less strain and therefore it is saved from rupturing.

It appears the most effective bactericidal surface was the polyDADMAC coated long needled bSi, with a cell death percentage of 54%. This was due to a combination of physical and chemical effects. These surface characteristics should be tested on alternative media.

## 6 Further Work

---

The beneficial implications of this project provide a basis for future work to improve these surfaces further. The factors found to optimise the bactericidal properties of a nanostructure surface may even be used on surfaces similar to those described in section 1.6 such as brush and niche type titania surfaces.

However, some of these factors may need to be refined and explained further. One of the main problems encountered was whether or not these surfaces are successful against gram-negative bacteria and not gram-positive or whether it's motility is the leading factor. To answer this, bacteria such as *K. pneumonia* (gram-negative, non-motile) and *B. subtilis* (gram-positive, motile) should also be used on the surface to test their effectiveness.

The qualitative results found from the polymer coated surfaces do not prove whether the chemical killing mechanism is from the residual NaCl ions or the polyDADMAC. In order to prove this either the surfaces can be fully washed, while XPS or optical microscopy can be used to visualise any micelles being expelled from the cell wall.

## 7 References

---

- [1]. S.A. Onaizi and S. S. Leong, *Biotechnol. Adv.* 2011, **29**, 67-74
- [2]. A.G. Gristina, *Science*, 1987, **237**, 1588-95
- [3]. R. O. Darouchie, *N Engl J Med*, 2004, **350**, 1422-9
- [4]. H. Shah, W. Bosch, K. M. Thompson and W. C. Hellinger, *Neurohospitalist*, 2013, **3**, 144-151
- [5]. N. J. Hickok and I. M. Shapiro, *Adv Drug Deliv Rev*, 2012, **64**, 1165-76
- [6]. D. Campoccia, L. Montanaro and C. R. Arciola, *Biomaterials*, 2013, **34**, 8018-29
- [7]. J. Zhang, K. G. Neoh, X. Hu, E. T. Kang, *Biomaterials*, 2014, **35**, 7690-8
- [8]. M. J. G. Minier, M. Salmain, N. Yacoubi and C. Pradier, *Langmuir*, 2005, **21**, 5957-65
- [9]. A. J. Huh and Y. J. Kwon, *J Control Release*, 2011, **156**, 128-45
- [10]. M. B. Avison, *Biology*, 2005, **6**, 243
- [11]. J. M. A. Blair, M. A. Webber, A. J. Baylay, D. O. Ogbolu and L. J. V. Piddock, *Nature Rev Microbiol*, 2015, **13**, 42-51
- [12]. J. A. Wu, C. Kusuma, J. J. Mond and J. F. Kokai-Kun, *Antimicrob Agents Chemother*, 2003, **47**, 3407-14.
- [13]. O'Neill, J., Securing new drugs for future generations: the pipeline of antibiotics. London: Wellcome Trust, 2015.
- [14]. T. Wagner, C. Neinhuis, W. Barthlott, *Acta Zool.*, 1996, **77**, 213.
- [15]. E.P Ivanova, J. Hasan, H. K. Webb, V. K. Truong, G. S. Watson, J. A. Watson, V. A. Baulin, S. Pogodin, J. Y. Wang, M. J. Tobin, C. Lobbe, and R. J. Crawford, *Small*, 2012, **8**, 2489-2494.
- [16]. Y.C. Jung, B. Bhushan, *Langmuir*, 2009, **25**, 14165
- [17]. L. Wen, J. C. Weaver, G. V. Lauder, *J. Exp. Biol.*, 2014, **217**, 1656-1666.
- [18]. W. Barthlott, C. Neinhuis, *Planta*, 1997, **202**, 1.
- [19]. C. Darwin, *On the Origin of Species by Means of Natural Selection*, John Murray, London, 1895.
- [20]. H. M. Hu, J. A. Watson, B. W. Cribb, G. S. Watson, *Biofouling*, 2011, **27**, 1125.
- [21]. E. E. Mann, D. Manna, M. R. Mettetal, R. M. May, E. M. Dannemiller, K. K. Chung, A. B. Brennan, S. T. Reddy, *Antimicrob Resist. Infect. Control*, 2014, **3**, 28
- [22]. A. Sakamoto, Y. Terui, C. Horie, T. Fukui, T. Masuzawa, K. Shigeta, K. Igarashi, K. Kashiwagi, *FEMS Microbiol. Lett.*, 2015, **361**, 10-16.
- [23]. J. Hasan, R. J. Crawford, E.P Ivanova, *Trends in Biotechnol.*, 2013, **31**, 295-304.

- [24]. J. Hasan, H.K. Webb, S. Pogodin, V.A. Baulin, G.S. Watson, J.A. Watson, R.J. Crawford, E.P. Ivanova, *Appl. Microbiol. Biotechnol.*, 2013, **97**, 9257-9262.
- [25]. E.P. Ivanova, J. Hasan, H. K. Webb, G. Gervinskas, S. Juodkazis, V. K. Truong, A. H. F. Wu, R. N. Lamb, V. A. Baulin, G. S. Watson, J. A. Watson, D. E. Mainwaring, R. J. Crawford, *Nat. Commun.*, 2013, **4**, 2838.
- [26]. S. Baker, C. Griffiths, J. Nicklin, *Microbiology*, Garland Science, London, 4<sup>th</sup> edn, 2011, 51-56.
- [27]. B. Grubor, D. K. Meyeholz and M. R. Ackermann, *Vet. Pathol.* 2006, **43**, 595-612.
- [28]. A. Pierres, A. Benoiel, D. Touchard, P. Bongrand, *Biophys. J.*, 2008, **94**, 4114-4122.
- [29]. F. Xue, J. Liu, L. Guo, L. Zhang, Q. Li, *J. Theor. Biol.*, 2015, **385**, 1-7.
- [30]. R. J. Crawford, H. K. Webb, V. K. Truong, J. Hasan, E. P. Ivanova, *Adv. Colloid Interface Sci.*, 2012, **179-182**, 142-149
- [31]. P. Decuzzi, M. Ferrari, *Biomater.*, 2010, **31**, 173-179.
- [32]. G. O'Toole, and G. C. L. Wong, *Curr Opin Microbiol.*, 2016, **30**, 139-146.
- [33]. D. Perera-Costa, J. M. Bruque, M. L. Gonzalez-Martin, A. C. Gomez-Garcia, V. Vadillo-Rodriguez, *Langmuir*, 2014, **30**, 4633-4641
- [34]. M. Clegg, MSci Dissertation, University of Bristol, 2016.
- [35]. L. E. Fisher, Y. Yang, M Yuen, W. Zhang, *Biointerphases*, 2016, **11**, 011014-1.
- [36]. T. Diu, N. Faruqui, T. Sjostrom, B. Lamarre, H. F. Jenkinson, B. Su, M. G. Ryandnov, *Sci. Rep.*, 2014, **4**, 7122.
- [37]. P.W. May, M. Clegg, T. A. Silva, H. Zanin, O. Fatilbello, V. Celorrio, D. J. Fermin, C. C. Welch, G. Hazell, L. Fisher, A. Nobbs, B. Su, *J. Mater. Chem. B.*, 2016, **4**, 5737-5746.
- [38]. S. Kalem, P. Werner, O. Arthursson, V. Talaaev, B. Nilsson, M. Hagberg, H. Frederiksen and U. Sodervall, *Nanotechnol.*, 2011, **22**, 253307.
- [39]. H. Jansen, M. de Boer, R. Legtenberg, M. Elwenspoek, *J. Micromech. Mircoeng.*, 1995, **5**, 115-120.
- [40]. B. Garipcan, S. Odabas, G. Demirel, J. Burger, S. S. Nonnenmann, M. T. Coster, E. M. Gallo, B. Nabet, J. E. Spanier and E. Piskin, *Adv Eng Mater*, 2010, **13**, 1-2
- [41]. P. W. May, *Phil. Trans. R. Soc. Lond. A.*, 2000, **358**, 473-495.
- [42]. P. Atkins, T. Overton, J. Rourke, M. Weller, F. Armstrong, *Shriver & Atkins' Inorganic Chemistry*, Oxford University Press, Oxford, 5<sup>th</sup> edn. 2010.
- [43]. N. N. Greenwood, A. Earnshaw, *Chemistry of the Elements*, Butterworth Heinemann, Oxford, 2<sup>nd</sup> edn., 2001, 272-278.
- [44]. L. Tang, C. Tsai, W. W. Gerberich, L. Kruckeberg and D. R. Kania, *Biomaterials*, 1995, **16**, 483-488

- [45]. D. H. Nguyen, V. T. H. Pham, M. A. Kobaisi, C. Bhadra, A. Orłowska, S. Ghanaati, B. M. Manzi, V. A. Baulin, S. Joudkazis, P. Kingshott, R. J. Crawford, E. P. Ivanova, *Langmuir*, 2016, **32**, 10744-10751.
- [46]. Sigma Aldrich, <http://www.sigmaaldrich.com/life-science/biochemicals/biochemical-products.html?TablePage=103994917> (accessed 16/11/16).
- [47]. Sigma Aldrich, <http://www.sigmaaldrich.com/technical-documents/articles/biofiles/fibronectin.html> (accessed 16/11/16).
- [48]. C. Brunot, L. Ponsonnet, C. Lagneau, P. Farge, C. Picart, B. Grosogeat, *Biomaterials*, 2007, **28**, 632-640
- [49]. K. Kabza, J. E. Gestwicki, and J. L. McGrath, *J. Chem. Educ.*, 2000, **77**, 63.
- [50]. S. Praver and R. J. Nemanich, *Philos. Trans. R. Soc. London.*, 2004, **362**, 2537
- [51]. J. Drelich, *Surface Innovations*, 2013, **1**, 248-254
- [52]. D. Mattia, H. H. Bau, Y. Gogotsi, *Langmuir*, 2006, **22**, 1789-1794
- [53]. R. R. Thomas, F. B. Kaufman, J. T. Kirleis and R. A. Belsky, *J. Electrochem Soc*, 1996, **143**, 643-8
- [54]. Z. Hu, H. Metiu, *J. Phys. Chem. C*, 2011, **115**, 17898-17909.
- [55]. *Dekker Encyclopaedia of Nanoscience and Nanotechnology*, J. A. Schwarz, C. I. Constescu, K. Putyera, Marcel Dekker, Inc. New York, 2004, 3331-33404.
- [56]. P. Stiefel, S. Schmidt-Emrich, K. Maniura-Weber, and Q. Ren, *BMC Microbiology*, 2015, **15**, 36.
- [57]. H. Persson, Z. Li, J. O. Tegenfeldt, S. Oredsson, and C. N. Prinz, *Sci. Rep*, 2015, **5**, 18535.
- [58]. M. Hajmeer, E. Ceylan, J. L. Marsden and D. Y. C. Fung, *Food Microbiol*, 2006, **23**, 446-452
- [59]. P. Gilbert and L. Moore, *J Appl Microbiol*, 2005, **99**, 703-15
- [60]. A. Mikhaylova, B. Leisenfield, D. Moore, W. Toreki, J. Vella, C. Batich and G. Shultz, *Wounds*, 2011, **23**, 24-31